A Content-Based Active Set Method for the Pressure Dependent Model of Water Distribution Systems

Jochen Deuerlein, Olivier Piller, Sylvan Elhay, Angus Simpson

Author-produced version of the article published in Journal of Water Resources Planning and Management, 145(1), 04018082. The original publication is available at https://ascelibrary.org/doi/abs/10.1061/(ASCE)WR.1943-5452.0001003.

A Content-Based Active Set Method for the Pressure Dependent Model of Water Distribution Systems

Jochen W. Deuerlein[1] Olivier Piller[2] Sylvan Elhay[3] Angus R. Simpson, M.ASCE[4]

October 22, 2018

Abstract

A new content based, box constrained, active set projected Newton method is presented which solves for the heads, the pipe flows and the nodal outflows of a water distribution system in which nodal outflows are pressure dependent. The new method is attractive because, by comparison with the weighted least squares energy and mass residuals (EMR) damped Newton method previously published by the authors, (i) it typically takes fewer iterations, (ii) it does not require damping, (iii) it takes less wall-clock time, (iv) it does not require the addition of any virtual elements and (v) it is algorithmically easier to deal with. Various pressure outflow relationships (PORs), which model nodal outflows, are considered and two new PORs are presented. The new method is shown, by application to eight previously published case study networks with up to about 20,000 pipes and 18,000 nodes, to be up to 5 times faster than the EMR method and to take between 34% and 70% fewer iterations than the EMR method.

Keywords: Active set method; Water distribution systems; Pressure dependent analysis; Pressure outflow relations; Content model; Karush-Kuhn-Tucker conditions

INTRODUCTION

Water engineers are frequently required to find the hydraulic steady-state pipe flows and nodal heads of water distribution system (WDS) models by solving the set of non-linear equations which model the energy and mass balance within the system under some known water demand requirements. The Newton methods that are typically used to solve WDSs are particularly suitable for demand driven models (DDMs) because (i) the derivatives in the system exist everywhere, (ii) the Jacobian is very sparse, (iii) the existence and uniqueness of the solution is guaranteed in many cases, and (iv) in most cases the convergence is quadratic (meaning that, asymptotically, the number of correct decimal digits approximately doubles at every iteration (Isaacson & Keller 1966, 95)). However, slow convergence or convergence failure (e.g. because of overshooting) can occur if the hydraulic equations involve sublinear functions (Piller et al. 2017). Examples of sublinear functions include (i) the inverse head loss formulae involved in the nodal method (Todini & Rossman 2013), (ii) the orifice equation for leakage outflow prediction and (iii) the inverse power outflow relation (POR) with an exponent greater than one. Various authors have addressed these problems, with some success, by introducing an underelaxation factor in the Newton iterations (Todini & Rossman 2013, Siew & Tanyimboh 2012, Giustolisi et al. 2008, Piller & Van Zyl 2007, Piller et al. 2003, Jun & Guoping 2013). Even so, the interest in pressure dependent models (PDMs), where the flow delivered to a network node is determined by the nodal pressure, has arisen because the simpler DDMs sometimes have solutions that are mathematically correct but not physically realizable.

The PORs (or consumption functions) used in PDMs determine the levels of delivery at nodes when the nodal pressures are insufficient to satisfy the nominal demands (i.e. the demands that would ideally be delivered): the POR sets delivery at zero for pressure heads smaller than a minimum pressure head, it sets delivery at

[1]Senior Researcher, 3S Consult GmbH, Albtalstrae 13, D 76137 Karlsruhe, Germany & Adjunct Senior Lecturer, School of Civil, Environmental and Mining Engineering, University of Adelaide, South Australia, 5005.

[2]Senior Research Scientist, Irstea, Water Department, Bordeaux Regional Centre, Cestas F-33612, France.

[3]Visiting Research Fellow, School of Computer Science, University of Adelaide, South Australia, 5005, sylvan.elhay@adelaide.edu.au.

[4]Professor, School of Civil, Environmental and Mining Engineering, University of Adelaide, South Australia, 5005.

the nominal demand d if the pressure head is higher than a prescribed maximum and between those levels for positive pressure heads which are insufficient to deliver the full nominal demand. PDM problems were given a sound theoretical underpinning with the observation of Deuerlein (2002) that for almost all of the relevant elements of a WDS model (including PDM nodes) a strictly monotone subdifferential mapping between flow and head loss, or in the case of a POR , between the outflow and the pressure, can be identified, ensuring that the corresponding content and co-content functions are strictly convex and thereby guarantee uniqueness of the solution.

The fact that PDM methods require a POR adds complexity to the solution process and convergence problems quickly became evident on even small PDM problems in the early days of pressure dependent modelling. Thus, a robust and rapidly convergent method which solves the PDM problem was presented in Elhay et al. (2016). That method can be considered the PDM counterpart of the Global Gradient Method (GGA) for the DDM problem and its success stems from the use of a Weighted Least Squares (WLS) optimization formulation combined with the line search algorithm of Goldstein (1967). The resulting damped Gauss-Newton method, which can be referred to as the energy and mass residuals (EMR) method, overcomes the poor convergence or convergence failures associated with the undamped Newton method for such problems and was found to reliably solve even quite challenging PDM problems rapidly. An important feature of the EMR method is that it uses an algorithm for which convergence can be mathematically proved.

The widely-used WDS solver, EPANET (Rossman 2000), uses head loss formulae which have a linear or superlinear (q^2) dependence on flow, q. Using a POR to determine the delivery at the nodes can introduce a sublinear element. In such cases convergence can suffer if the head and flow estimates in the iterative process that solves the nonlinear equations are far from the solution (Piller et al. 2017). Hence the need for damping.

Lippai & Wright (2014)) modelled PDM nodes by adding the following virtual elements: flow control valve (FCV), throttle control valve (TCV), link with a check valve (CV) and a reservoir to the network for each PDM node to produce a virtual controls equivalent network. More recently a similar approach was presented by Mahmoud et al. (2017). They connected control devices only to those nodes that a previously run DDM simulation identified as being in a PDM condition. These changes introduce only superlinear characteristics and, apart from extreme conditions, usually result in good convergence. The disadvantage of these approaches is that each such circumvention entails the addition of up to four elements per PDM node and can quickly lead to very large increases in the total number of degrees of freedom in the model. The significance of this increase is evident from the numbers in Table 1 which show the link, node and source counts for eight virtual control networks that are the equivalents of eight case study networks considered later in this paper. Columns 2–4 of Table 1 show the numbers of pipes, n_p, nodes, n_j and sources n_f in the actual networks. Columns 5–7 show, for the virtual controls equivalent networks, the number of links (pipes and virtual control valves), $n_p^v + n_c^v$, the number of nodes, n_j^v, the number of sources, n_f^v. The significant increase in the size of the network problem that has to be solved is seen in the ratios $(n_p^v + n_c^v)/n_p$, n_j^v/n_j and n_f^v/n_f. In addition to the huge increases in the numbers of links, nodes and sources (between 211 and 369% more links, between 176 and 300% more nodes and between 6,025 and 102,313% more sources), the equivalent virtual system may require the large extra computational cost of checking the states (at each iteration) of the extra virtual valves that are not in the original system (more than 30,600 for the case of network N_8). The technique of Mahmoud et al. (2017) is more economical but still increases the number of degrees of freedom in the model significantly.

In this paper a new content-based alternative to the EMR method is presented. This method, which solves for the nodal outflows as well as pipe flows and nodal heads, uses an Active Set Method (Hager & Zhang 2006) and will be referred to by the acronym ASM. The content-based optimization of the ASM formulation has only box constraints while the EMR method optimization has linear constraints which require selective projection methods (see Elhay et al. (2016) for EMR details and Hager & Zhang (2006) for a detailed discussion of this topic) which are harder to deal with. Moreover, the new method does not require the addition of any control devices. The new method is also attractive because it typically takes fewer steps than the EMR method. Importantly, the ASM does not, unlike the EMR, require any damping to rapidly converge to the required solution (apart from ill-posed problems caused, for example, by extremely high resistances or zero flows with the Hazen-Williams head loss model). The new formulation, being purely a content formulation, does not include any sublinear functions. Not requiring damping gives this approach a significant performance advantage. The authors' experience, discussed later, is that the ASM takes significantly less wall-clock time than the EMR, and this is particularly pronounced on large problems. Formal speed testing (something which is beyond the scope or intent of this paper) would need to be done to confirm this.

The new method has been implemented as part of the SIR 3S software suite (www.3sconsult.com.de) and successfully demonstrated as part of the ResiWater Project (ResiWater 2018) on networks with more than 50,000 pipes, although no details of that project are reported in this paper.

The iterative algorithm for the new ASM has three block equations. The one which determines the updated flows is precisely the same as the flows block equation for the EMR. The one which updates the heads is the same as the block equation for the heads in the EMR but with an additional term that involves the outflows. The third is a new equation which updates the outflows. This feature means that it is easy, should the need arise, to switch from the ASM to the EMR method by simply using only the flow update equation and head update equation with the outflow term omitted.

A number of PORs have appeared in the literature on pressure dependent models (Wagner et al. 1988, Fujiwara & Ganesharajah 1993, Gupta & Bhave 1996, Germanopoulos 1985).

More recently, Shirzad et al. (2013) studied a variety of POR models and evaluated them against measurements from field and laboratory tests. Their conclusion was that the Wagner POR performed best against their data. One of the PORs they studied is the sigmoid function which is used to model biological and physical phenomena which have exponential growth that saturates at some point. The logistic sigmoidal POR, which derives from the inverse of the logit function (Cramer 2003), was introduced to water distribution by Tanyimboh & Templeman (2004) to improve on POR models which have discontinuities in their derivatives at minimum and service pressure head points: discontinuities which can cause convergence difficulties if they are not addressed. Later, Ciaponi et al. (2015) proposed a Monte-Carlo methodology in which a POR is based on demand flow simulations in building environments. Internally, the Wagner POR was used at tap flows but after aggregation a family of sigmoid-shaped curves better fitted the simulation results. Their motivation was to provide a physical basis for the development of PORs. They recommend the logistic sigmoidal POR for its smoothness and its sigmoid shape which matches their simulation results. Even so, further research in this area is warranted.

The algorithm for the new method requires slight refinements for some PORs because of the behaviour of those consumption functions at the points of minimum and service pressure heads. This is because the method uses the POR and its derivative and the inverse POR and its derivative. For example, the derivative of the Wagner et al. (1988) POR is undefined at zero and this can cause convergence difficulties in some cases and so a refinement, discussed below and called "derivative assignment", is presented which overcomes this difficulty. Similarly, the inverse of the logistic sigmoidal POR is an affine transformation of the logit function and as a consequence it and its inverse are not defined at 0 and d, the nominal nodal demand. Further, the zero derivatives at the points of minimum and service pressure heads of the cubic POR of Fujiwara & Ganesharajah (1993) and the 2-side regularized Wagner POR of Piller et al. (2003) mean that their inverses have infinite derivatives for values of the outflows at 0 and d. A simple interval reduction strategy is described later which overcomes these potential numerical problems.

The examples used to illustrate the effectiveness of the new method use a new POR which is introduced: the 1-side regularized Wagner POR. This POR has a small quadratic regularization segment near the origin to give it a non-infinite derivative at 0. A second new POR, called the "quadratic" POR is also introduced. The convergence behaviour of the new method is, in the experience of the authors, remarkably similar for all the PORs tested, although, of course, the delivery fractions differ between the PORs. Table 2 lists the formulae for the functional form of several PORs in terms of the head fraction z, defined in (1), for $z \in [0, 1]$.

The rest of this paper is organized as follows. The next section introduces some definitions and notation and briefly gives an overview of the PORs considered, the following section introduces the PDM content model and the section following that develops the active set method which is the main contribution of the paper. The next section discusses some implementation issues such as initialization, stalled iterations and termination, derivative assignment and interval reduction and the section following that presents some examples of solution by the ASM of a small illustrative example and a summary of the comparison between the performance of the EMR method and the ASM. The solution of the eight case study networks considered in Elhay et al. (2016) is then used to illustrate the faster convergence of the ASM over the EMR method. A brief report is presented on the efficacy of the derivative assignment technique where the unregularized Wagner POR is used with the ASM and the use of interval reduction for the cubic, logistic and 2-side regularization Wagner PORs is briefly discussed. An appendix details some of the PORs discussed, their derivatives, their inverses and the derivatives of their inverses.

DEFINITIONS AND NOTATION

Consider a WDS whose network graph has n_p links, or arcs, and $n_j + n_f$ nodes, or vertices: n_j is the number of nodes at which the heads are unknown and $n_f \geq 1$ is the number of source nodes with fixed heads. The links of the network include valves, pumps and pipes but in this paper networks with only pipes will be considered. However, all the results extend naturally to networks with pumps and valves.

Denote by $\boldsymbol{q} = (q_1, q_2, \ldots, q_{n_p})^T \in \mathbb{R}^{n_p}$ the vector of unknown flows in the system, $\boldsymbol{h} = (h_1, h_2, \ldots, h_{n_j})^T \in \mathbb{R}^{n_j}$ the unknown heads at the nodes in the system, $\boldsymbol{u} = (u_1, u_2, \ldots, u_{n_j})^T \in \mathbb{R}^{n_j}$ the vector of node elevations and $\boldsymbol{r}(\boldsymbol{q}) = (r_1, r_2, \ldots, r_{n_p})^T$ the vector of pipe resistance factors. Let $\boldsymbol{A}$ denote the $n_p \times n_j$, full rank, unknown-head arc-node incidence matrix, (ANIM): $[\boldsymbol{A}]_{ji} = -1$ if node i is at the end of arc j, 0 if arc j does not connect to the node i and 1 if arc j starts at node i. Let $\boldsymbol{A}_f$ denote the ANIM, with a similar definition, for the fixed-head nodes. Let $\boldsymbol{h}^0$ denote the vector of elevations of the n_f fixed-head nodes. Denote $\boldsymbol{a} = \boldsymbol{A}_f \boldsymbol{h}^0$. Denote by α the exponent used in the head loss formula: $\alpha = 2$ for the Darcy-Weisbach model and $\alpha = 1.852$ for the Hazen-Williams model. Furthermore, denote by $\boldsymbol{G}(\boldsymbol{q}) \in \mathbb{R}^{n_p \times n_p}$ the diagonal matrix whose diagonal elements are defined as $[\boldsymbol{G}(\boldsymbol{q})]_{jj} = r_j |q_j|^{\alpha - 1}$. Then, $\boldsymbol{\xi}(\boldsymbol{q}) = \boldsymbol{G}(\boldsymbol{q})\boldsymbol{q}$ is the vector whose elements model the head losses of the pipes in the system. In general, (e.g. for the Darcy-Weisbach formula) $\boldsymbol{r} = \boldsymbol{r}(\boldsymbol{q})$ but for the Hazen-Williams formula $\boldsymbol{r}$ is independent of $\boldsymbol{q}$. Denote the vector of the given demands at the nodes with unknown-head by $\boldsymbol{d} = (d_1, d_2, \ldots, d_{n_j})^T \in \mathbb{R}^{n_j}$. Denote by $\boldsymbol{c}(\boldsymbol{h}, \boldsymbol{d}) \in \mathbb{R}^{n_j}$ the vector whose elements are the consumption function values at the n_j nodes of the system. Throughout what follows, the symbol $\boldsymbol{O}$ denotes a zero matrix and $\boldsymbol{o}$ denotes a zero column vector of appropriate dimension for the particular case. The shorthand notation $\boldsymbol{x} + a$, where $\boldsymbol{x}$ is a vector and a is a scalar, will be used to denote the case where every component of $\boldsymbol{x}$ has a added to it. Furthermore, it will be assumed that any matrix inverses which are shown do exist.

Turning now to PDM problems, assume, for simplicity and without loss of generality, that every node has the same minimum pressure head, h_m, and the same service pressure head, h_s. Denote a node's elevation by u and define the pressure fraction, $z(h)$, by

$$z(h) = \frac{(h - (h_m + u))}{(h_s - h_m)}. \tag{1}$$

Suppose that $\gamma(t)$ is a bounded, smooth, monotonically increasing function which maps the interval $[0, 1] \to [0, 1]$. In this paper, the POR at a node is defined by

$$c(h) = \begin{cases} 0 & \text{if } z(h) \leq 0 \\ d\,\gamma(z(h)) & \text{if } 0 < z(h) < 1 \\ d & \text{if } z(h) \geq 1 \end{cases}. \tag{2}$$

Previously considered POR functions include the linear POR (Elhay et al. 2016), the cubic POR of Fujiwara & Ganesharajah (1993), the Heaviside (step function) POR of Bhave (1981) and later Piller & Van Zyl (2007), the Wagner POR of Wagner et al. (1988), the 2-side regularized Wagner POR of Piller et al. (2003) and the logistic sigmoidal POR of Tanyimboh & Templeman (2004).

The inverse function of the POR, the head, $h(c)$ expressed as a function of outflow c, will be required for the development of the active set method (ASM) which is the subject of this paper. But, the function $h(c)$ is not in general everywhere differentiable and so in its place a multivalued, sub-differential mapping is considered:

$$h(c) = \begin{cases} \emptyset & \text{if } c < 0 \\ (-\infty, h_m + u] & \text{if } c = 0 \\ (h_s - h_m)\gamma^{-1}\left(\frac{c}{d}\right) + h_m + u & \text{if } 0 < c < d \\ [h_s + u, +\infty) & \text{if } c = d \\ \emptyset & \text{if } c > d \end{cases}. \tag{3}$$

A full discussion of PORs is deferred until after the ASM has been developed and its algorithm presented. However, we note here that two new PORs are introduced in this paper: (i) $c_s(h)$, a 1-side regularized Wagner POR and (ii) $c_2(h)$, a quadratic POR which closely follows the unregularized Wagner POR. Importantly, both of these new PORs have bounded derivatives for $z \in [0, 1]$ and their inverses have bounded derivatives for $c \in [0, d]$. The 1-side regularized Wagner POR, $c_s(z)$, and its inverse, $h_s(c)$, are shown in Fig. 3. The quadratic POR, $c_2(z)$, is shown in Fig. 4 together with the unregularized Wagner POR, $c_w(z)$. The maximum point-wise difference between the two curves is $\max_{z \in [0,1]} |c_2(z) - c_w(z)| < 0.15$. The Heaviside, or step function POR is defined by $c(h) = 0$ if $h < h_m$ and d otherwise. It's structure means that the proofs by which the existence and

uniqueness of the other PORs can be shown do not apply. Even so, the existence and uniqueness of a solution can be established as will be seen later.

Where pressure dependent systems have been simulated by adding four model elements to every demand node in a network, the elevation of the reservoir is set to the minimum pressure head, h_m, the FCV is set to the nominal nodal demand d and the minor loss coefficient of the TCV is chosen so that the head loss for the flow $c = d$ is set at the service pressure head, h_s. The inverse POR function $h(c)$ can be thought of as the head loss function on the pseudo links in such an arrangement. This approach was first used in EPANET models. It has the significant disadvantage that it greatly increases the dimension of the problem. Fig. 5 shows such an arrangement for a demand node.

The Appendix lists the formulae for the linear, quadratic, unregularized Wagner, 1-side Regularized Wagner, logistic sigmoidal and Heaviside PORs, their derivatives, their inverses and the derivatives of their inverses. The five inverse POR sub-differential mappings for the inverse linear, $h_1(c)$, inverse quadratic, $h_2(c)$, inverse unregularized Wagner, $h_w(c)$, inverse 1-side regularized Wagner, $h_s(c)$, logistic sigmoidal, $h_\sigma(c)$, and inverse Heaviside, $h_h(c)$, functions are shown in Fig. 6. The dashed line shows the regularizing quadratic portion of $h_s(c)$. On the rest of the interval $h_s(c)$ and $h_w(c)$ are identical.

In this paper the minimization of the content function is achieved by an active set, projected Newton method that examines the KKT conditions at each iteration. Unlike pure projection methods, where the same the projection is used until convergence and then adapted, in the new method the projection onto the feasible set can change significantly at each iteration. Convergence occurs in spite of these large changes.

THE PDM CONTENT MODEL

It was shown in Elhay et al. (2016) that if the PDM content function $C(\boldsymbol{q})$ is defined by

$$C(\boldsymbol{q}) = \sum_{j=1}^{n_p} \int_0^{q_j} \xi_j(s)ds - \boldsymbol{a}^T\boldsymbol{q} + \sum_{i=1}^{n_j} \int_0^{-\boldsymbol{e}_i^T\boldsymbol{A}^T\boldsymbol{q}} h(s)ds \tag{4}$$

and the set U is defined by $U = \{\boldsymbol{q} \in \mathbb{R}^{n_p} | \boldsymbol{o} \le -\boldsymbol{A}^T\boldsymbol{q} \le \boldsymbol{d}\}$ then the problem of finding $\min_{\boldsymbol{q}\in U} C(\boldsymbol{q})$ is associated with a Lagrangian which can, after some rearrangement, be written as $L(\boldsymbol{q},\boldsymbol{h}) = \sum_{j=1}^{n_p}\int_0^{q_j}\xi_j(s)ds - \boldsymbol{a}^T\boldsymbol{q} - \boldsymbol{h}^T\boldsymbol{A}^T\boldsymbol{q} - \sum_{i=1}^{n_j}\int_{h_m}^{h_i} c(s)ds$ and this leads to the unconstrained but equivalent problem of finding $\min_q \max_h L(\boldsymbol{q},\boldsymbol{h})$. The gradient of $L(\boldsymbol{q},\boldsymbol{h})$ is $\boldsymbol{f}(\boldsymbol{q},\boldsymbol{h}) = \begin{pmatrix} \boldsymbol{G}(\boldsymbol{q})\boldsymbol{q} - \boldsymbol{A}\boldsymbol{h} - \boldsymbol{a} \\ -\boldsymbol{A}^T\boldsymbol{q} - \boldsymbol{c}(\boldsymbol{h}) \end{pmatrix} \stackrel{\text{def}}{=} \begin{pmatrix} \boldsymbol{\rho}_e \\ \boldsymbol{\rho}_m \end{pmatrix}$ and the PDM steady-state heads and flows are found as the solution of $\boldsymbol{f}(\boldsymbol{q},\boldsymbol{h}) = \boldsymbol{o}$. Here $\boldsymbol{\rho}_e$ is the energy residual and $\boldsymbol{\rho}_m$ is the mass balance residual.

Replacing $-\boldsymbol{e}_j^T\boldsymbol{A}^T\boldsymbol{q}$ by c_j in the last term of (4) allows the definition of a convex and lower semi-continuous demand-node content function which is associated with the sub-differential mapping in (3):

$$\overline{W}(c_i) = \begin{cases} \infty & \text{if } c_i < 0 \\ (h_m + u_i)c_i + (h_s - h_m)\int_0^{c_i} \gamma^{-1}\left(\frac{x}{d_i}\right)dx & \text{if } 0 \le c_i \le d_i, \quad d_i > 0\,. \\ \infty & \text{if } c_i > d_i \end{cases} \tag{5}$$

The function $\overline{W}$ takes the special form $(h_m + u_i)c_i$ as proposed in Piller & Van Zyl (2007) for the Heaviside POR. The Jacobian of $\boldsymbol{f}$ is $\nabla_{\boldsymbol{q},\boldsymbol{h}}\boldsymbol{f}(\boldsymbol{q},\boldsymbol{h}) = \begin{pmatrix} \boldsymbol{F}(\boldsymbol{q}) & -\boldsymbol{A} \\ -\boldsymbol{A}^T & -\boldsymbol{E}(\boldsymbol{h}) \end{pmatrix}$ where $\boldsymbol{F}(\boldsymbol{q})$ and $\boldsymbol{E}(\boldsymbol{h})$ are diagonal matrices which are such that (i) the terms on the diagonal of $\boldsymbol{F}(\boldsymbol{q})$ are the q-derivatives of the corresponding terms in $\boldsymbol{G}(\boldsymbol{q})\boldsymbol{q}$ and (ii) the terms on the diagonal of $\boldsymbol{E}$ are the h-derivatives of the corresponding terms in $\boldsymbol{c}(\boldsymbol{h})$. The steady-state heads and flows are found in Elhay et al. (2016) by a Goldstein line-search, damped Newton method which uses this Jacobian.

The corresponding development for the DDM case has (i) the POR replaced by the constant, nominal demands $\boldsymbol{d}$, (ii) the corresponding replacement of the submatrix $\boldsymbol{E}(\boldsymbol{h})$ by a zero matrix and (iii) the last term in (4) omitted. The Newton method for the steady-state solutions in the DDM case do not usually require damping.

AN ACTIVE SET METHOD FOR THE CONTENT MODEL

In this section an active set formulation of this problem is developed which usually requires no damping and which, in most cases, requires fewer iterations. This method is a natural implementation of the

PDM content model and comes from expressing the head as a function of outflow c. Denote $\psi(c_i) = (h_s - h_m)\int_0^{c_i}\gamma^{-1}\left(\frac{x}{d_i}\right)dx, \quad d_i > 0$, denote $\boldsymbol{\psi}(\boldsymbol{c}) = (\psi(c_1), \psi(c_2), \ldots, \psi(c_{n_j}))^T$ and $\mathbf{1} = (1, 1, \ldots, 1)^T$. The total system content is, noting that $\overline{W}(c_i)$ of (5) is a function of c which is not constrained to have $\boldsymbol{c}$ equal to $-\boldsymbol{A}^T\boldsymbol{q}$, defined by $C(\boldsymbol{q}, \boldsymbol{c}) = \sum_{j=1}^{n_p}\int_0^{q_j}\xi_j(s)ds + \sum_{\substack{1\le i\le n_j \\ d_i>0}}\overline{W}(c_i) - \boldsymbol{a}^T\boldsymbol{q}$. The function $C(\boldsymbol{q}, \boldsymbol{c})$ is strictly convex and norm-coercive in $\boldsymbol{q}$ and $\boldsymbol{c}$ and this guarantees the existence and uniqueness of the solution provided the mass balance constraint is not empty. Now, $\overline{W}(c_j)$ in (5) is an unconstrained, convex, lower semi-continuous, sub-differentiable function but it can be replaced by a constrained differentiable function which is defined only for $0 \le c_i \le d_i$, leading to the total system content function $C(\boldsymbol{q}, \boldsymbol{c}) = \sum_{j=1}^{n_p}\int_0^{q_j}\xi_j(s)ds + \sum_{\substack{1\le i\le n_j \\ d_i>0}}\left\{(h_m + u_i)c_i + (h_s - h_m)\int_0^{c_i}\gamma^{-1}\left(\frac{s}{d_i}\right)ds\right\} - \boldsymbol{a}^T\boldsymbol{q}$. subject to $-\boldsymbol{A}^T\boldsymbol{q} - \boldsymbol{c} = \boldsymbol{o}, \ -\boldsymbol{c} \le \boldsymbol{o}, \ \boldsymbol{c} \le \boldsymbol{d}$. This content function is associated with the constrained minimization problem

$$\begin{gathered}\min_{q,c} C(\boldsymbol{q}, \boldsymbol{c}) = \min_{q,c}\left\{\sum_{j=1}^{n_p}\int_0^{q_j}\xi_j(s)ds - \boldsymbol{a}^T\boldsymbol{q} + \boldsymbol{c}^T(\boldsymbol{u} + h_m) + \sum_{\substack{1\le i\le n_j \\ d_i>0}}\psi(c_i)\right\} \\ \text{subject to } -\boldsymbol{A}^T\boldsymbol{q} - \boldsymbol{c} = \boldsymbol{o}, \quad -\boldsymbol{c} \le \boldsymbol{o}, \quad \boldsymbol{c} \le \boldsymbol{d}.\end{gathered} \tag{6}$$

An equivalent reduced form of the problem in (6) was proposed by Piller et al. (2003). The function C is, for the linear, 1-side regularized Wagner and quadratic PORs, strictly convex by virtue of the strict monotonicity of the head loss functions and it is also norm-coercive ($|C(\boldsymbol{q}, \boldsymbol{c})| \to \infty$ if $\|\boldsymbol{q}\|, \|\boldsymbol{c}\| \to \infty$. In order for a solution to exist it is only necessary that the polyhedral constraint set $-\boldsymbol{A}^T\boldsymbol{q} - \boldsymbol{c} = \boldsymbol{o}$ and $\boldsymbol{o} \le \boldsymbol{c} \le \boldsymbol{d}$ is non-empty. The pipe flows $\boldsymbol{q} = \boldsymbol{o}$ and nodal outflows $\boldsymbol{c} = \boldsymbol{o}$ are trivially feasible solutions for the constraint set and so the PDM problem consists of the minimization of a strictly convex content function formulated in terms of unknown flows $\boldsymbol{q}, \boldsymbol{c}$ over a polyhedral set.

The necessary, and in this case sufficient, conditions for a solution to the problem in (6) are given by the Karush-Kuhn-Tucker (KKT) conditions. The Lagrangian of (6) is

$$\begin{aligned}L(\boldsymbol{q}, \boldsymbol{c}, \boldsymbol{h}, \boldsymbol{\lambda}, \boldsymbol{\mu}) = \sum_{j=1}^{n_p}\int_0^{q_j}\xi_j(s)ds - \boldsymbol{a}^T\boldsymbol{q} + \mathbf{1}^T\boldsymbol{\psi}(\boldsymbol{c}) + \boldsymbol{c}^T(\boldsymbol{u} + h_m) - \boldsymbol{h}^T(\boldsymbol{A}^T\boldsymbol{q} + \boldsymbol{c}) \\ + \boldsymbol{\mu}^T(\boldsymbol{c} - \boldsymbol{d}) - \boldsymbol{\lambda}^T\boldsymbol{c} \ \text{ subject to } \boldsymbol{\lambda} \ge \boldsymbol{o}, \ \boldsymbol{\mu} \ge \boldsymbol{o}.\end{aligned} \tag{7}$$

Here $\boldsymbol{h}$ represents the Lagrange multipliers for the mass balance equality constraint and $\boldsymbol{\lambda}$ and $\boldsymbol{\mu}$ are the non-negative Lagrange multipliers for the inequality constraints in the outflows, $\boldsymbol{c}$. A constraint is said to be active or binding if it satisfies equality. Thus, if an outflow, c, is at zero or at the nominal demand d, the corresponding constraint would be said to be active.

The Lagrangian (7) has exactly one saddle point which minimizes L with respect to $\boldsymbol{q}, \boldsymbol{c}$ and maximizes L with respect to $\boldsymbol{h}, \boldsymbol{\lambda}, \boldsymbol{\mu}$. Suppose that $\boldsymbol{\lambda}^*$ and $\boldsymbol{\mu}^*$ are the Lagrangian multipliers of the active constraints. Setting to zero the derivative of L with respect to $\boldsymbol{q}, \boldsymbol{c}, \boldsymbol{h}, \boldsymbol{\lambda}^*, \boldsymbol{\mu}^*$ gives the necessary and, in this case, sufficient conditions for a minimum. Adding the complementary slackness conditions for the inequality constraints gives the so called KKT conditions.

If $\boldsymbol{\theta}(\boldsymbol{c})$ denotes the scaled vector of inverse POR functions $\boldsymbol{\theta}(\boldsymbol{c}) = \nabla_{\boldsymbol{c}}\boldsymbol{\psi}(\boldsymbol{c}) = (h_s - h_m)\left(\gamma^{-1}(c_1/d_1), \gamma^{-1}(c_2/d_2), \ldots, \gamma^{-1}(c_{n_j}/d_{n_j})\right)^T$ then, according to the KKT conditions, the minimum is achieved where

$$\boldsymbol{\xi}(\boldsymbol{q}) - \boldsymbol{A}\boldsymbol{h} - \boldsymbol{a} = \boldsymbol{o} \tag{8}$$

$$\boldsymbol{\theta}(\boldsymbol{c}) + \boldsymbol{u} + h_m - \boldsymbol{h} - \boldsymbol{L}^T\boldsymbol{\lambda}^* + \boldsymbol{U}^T\boldsymbol{\mu}^* = \boldsymbol{o} \tag{9}$$

$$-\boldsymbol{A}^T\boldsymbol{q} - \boldsymbol{c} = \boldsymbol{o} \tag{10}$$

$$-\boldsymbol{L}\boldsymbol{c} = \boldsymbol{o} \tag{11}$$

$$\boldsymbol{U}(\boldsymbol{c} - \boldsymbol{d}) = \boldsymbol{o} \tag{12}$$

where $\boldsymbol{L}$ is a matrix made up of rows of the identity whose indices correspond to those of the nodes at which the lower constraint is satisfied (or binding) and $\boldsymbol{U}$ is a matrix made up of rows of the identity whose indices correspond to those of the nodes at which the upper constraint is satisfied. Eq. (8) is the conservation of energy equation and (9) defines $\boldsymbol{h}$ according to (3). The Lagrange multipliers have a physical interpretation: $\mu_i = [h_i - u_i - h_s]^+$ represents the surplus pressure in the case of full supply at the node and $\lambda_i = [h_i - u_i - h_m]^-$

represents the missing deficit pressure in the case of zero supply. Fig. 7 shows three cases: (a) full delivery, (b) partial delivery and (c) failure mode. A value of $\lambda > 0$ (the case shown) indicates that the pressure deficit is λ and a value of $\mu > 0$ (the case shown) indicates a pressure surplus of μ.

Denote by $\boldsymbol{M}(\boldsymbol{c})$, or just $\boldsymbol{M}$, where there is no ambiguity, the diagonal matrix whose diagonal elements contain the $\boldsymbol{c}$ derivatives of the inverse POR function $\boldsymbol{h}(\boldsymbol{c})$ and recall that the matrix $\boldsymbol{F}$ denotes the diagonal matrix whose diagonal elements are q-derivatives of the corresponding terms in $\boldsymbol{G}(\boldsymbol{q})\boldsymbol{q}$. The Newton-Raphson iteration for this system takes the form

$$\begin{array}{c} \\ n_p \\ n_j \\ n_j \\ n_L \\ n_U \end{array} \begin{array}{c} \begin{array}{ccccc} n_p & n_j & n_j & n_L & n_U \end{array} \\ \begin{pmatrix} \boldsymbol{F}^{(m)} & \boldsymbol{O} & -\boldsymbol{A} & \boldsymbol{O} & \boldsymbol{O} \\ \boldsymbol{O} & \boldsymbol{M}^{(m)} & -\boldsymbol{I} & -\boldsymbol{L}^{(m)^T} & \boldsymbol{U}^{(m)^T} \\ -\boldsymbol{A}^T & -\boldsymbol{I} & \boldsymbol{O} & \boldsymbol{O} & \boldsymbol{O} \\ \boldsymbol{O} & -\boldsymbol{L}^{(m)} & \boldsymbol{O} & \boldsymbol{O} & \boldsymbol{O} \\ \boldsymbol{O} & \boldsymbol{U}^{(m)} & \boldsymbol{O} & \boldsymbol{O} & \boldsymbol{O} \end{pmatrix} \end{array} \begin{pmatrix} \boldsymbol{q}^{(m+1)} - \boldsymbol{q}^{(m)} \\ \boldsymbol{c}^{(m+1)} - \boldsymbol{c}^{(m)} \\ \boldsymbol{h}^{(m+1)} - \boldsymbol{h}^{(m)} \\ \boldsymbol{\lambda}^{(m+1)} - \boldsymbol{\lambda}^{(m)} \\ \boldsymbol{\mu}^{(m+1)} - \boldsymbol{\mu}^{(m)} \end{pmatrix} = \\ - \begin{pmatrix} \boldsymbol{G}^{(m)}\boldsymbol{q}^{(m)} - \boldsymbol{A}\boldsymbol{h}^{(m)} - \boldsymbol{a} \\ \boldsymbol{\theta}^{(m)} + \boldsymbol{u} + h_m - \boldsymbol{h}^{(m)} - \boldsymbol{L}^{(m)^T}\boldsymbol{\lambda}^{(m)} + \boldsymbol{U}^{(m)^T}\boldsymbol{\mu}^{(m)} \\ -\boldsymbol{A}^T\boldsymbol{q}^{(m)} - \boldsymbol{c}^{(m)} \\ -\boldsymbol{L}^{(m)}\boldsymbol{c}^{(m)} \\ \boldsymbol{U}^{(m)}(\boldsymbol{c}^{(m)} - \boldsymbol{d}) \end{pmatrix} \qquad (13)$$

The system (13) allows some immediate simplifications. The third block equation reduces to $\boldsymbol{\rho}_m^{(m+1)} = -\boldsymbol{A}^T\boldsymbol{q}^{(m+1)} - \boldsymbol{c}^{(m+1)} = \boldsymbol{o}$. Similarly, the fourth block equation reduces to $\boldsymbol{L}^{(m)^T}\boldsymbol{c}^{(m+1)} = \boldsymbol{o}$ and the last block equation reduces to $\boldsymbol{U}^{(m)}\boldsymbol{c}^{(m+1)} = \boldsymbol{U}^{(m)}\boldsymbol{d}$.

It is important to note that the matrices $\boldsymbol{U}^{(m)}$ and $\boldsymbol{L}^{(m)}$ are superscripted because the constraints which are active can change from one iteration to the next. Thus, after each iteration the Lagrange multipliers λ_i and μ_i are checked. A non-negative Lagrange multiplier indicates an active constraint. The matrices $\boldsymbol{U}^{(m+1)}$ and $\boldsymbol{L}^{(m+1)}$ are updated to include the all rows of the identity matrices which correspond to active constraints and if any of the Lagrange multipliers are negative the corresponding rows of the $\boldsymbol{U}^{(m+1)}$ and $\boldsymbol{L}^{(m+1)}$ are removed. Of course, only one of the two box constraints can be active at any one time. Note that the matrices $\boldsymbol{U}$ and $\boldsymbol{L}$ are not explicitly formed in the practical implementation of the active set method but they serve here to clarify the exposition.

The outflows for the nodes at which the constraints are active are no longer unknowns and so they can be moved to the right-hand-side of the system of equations. This reduces the dimension of the system to be solved. The details of this process are described in the Appendix. The resulting simplified system is then, with the selection matrix $\boldsymbol{B}^{(m)}$ is defined by $\boldsymbol{B}^{(m)} = \begin{array}{c} \\ n_b \end{array} \begin{array}{c} \begin{array}{ccc} n_b & n_l & n_u \end{array} \\ \begin{pmatrix} \boldsymbol{I} & \boldsymbol{O} & \boldsymbol{O} \end{pmatrix} \end{array}$,

$$\begin{array}{c} \\ n_p \\ n_b \\ n_j \end{array} \begin{array}{c} \begin{array}{ccc} n_p & n_b & n_j \end{array} \\ \begin{pmatrix} \boldsymbol{F}^{(m)} & \boldsymbol{O} & -\boldsymbol{A} \\ \boldsymbol{O} & \boldsymbol{M}_b^{(m)} & -\boldsymbol{B}^{(m)} \\ -\boldsymbol{A}^T & -\boldsymbol{B}^{(m)^T} & \boldsymbol{O} \end{pmatrix} \end{array} \begin{pmatrix} \boldsymbol{q}^{(m+1)} - \boldsymbol{q}^{(m)} \\ \boldsymbol{c}_b^{(m+1)} - \boldsymbol{c}_b^{(m)} \\ \boldsymbol{h}^{(m+1)} - \boldsymbol{h}^{(m)} \end{pmatrix} = - \begin{pmatrix} \boldsymbol{\rho}_e^{(m)} \\ \boldsymbol{\theta}_b^{(m)} - \boldsymbol{h}_b^{(m)} + h_m + \boldsymbol{u}_b \\ \boldsymbol{\rho}_m^{(m)} \end{pmatrix} \qquad (14)$$

where $\boldsymbol{M}_b$, $\boldsymbol{c}_b$, $\boldsymbol{\theta}_b$, $\boldsymbol{u}_b$ and $\boldsymbol{h}_b$ are the quantities which apply to those nodes at which the constraints are not active, i.e. those nodes where the outflows lie between the upper and lower bounds. The second block row equation of (14) involves only the nodes which have non-zero demands and are in a pressure deficient condition. The first block row equation of (14) can be rearranged to give

$$\boldsymbol{q}^{(m+1)} = \boldsymbol{q}^{(m)} - \boldsymbol{F}^{(m)^{-1}} \left(\boldsymbol{G}^{(m)}\boldsymbol{q}^{(m)} - \boldsymbol{A}\boldsymbol{h}^{(m+1)} - \boldsymbol{a} \right) \qquad (15)$$

and the second block row equation of (14) can be rearranged, provided the inverse of $\boldsymbol{M}_b^{(m)}$ exists, to give

$$\boldsymbol{c}_b^{(m+1)} = \boldsymbol{c}_b^{(m)} - \boldsymbol{M}_b^{(m)^{-1}} \left(\boldsymbol{\theta}_b^{(m)} - \boldsymbol{h}_b^{(m+1)} + h_m + \boldsymbol{u}_b \right). \qquad (16)$$

Denoting $\boldsymbol{E}^{(m)} = \boldsymbol{B}^{(m)^T}\boldsymbol{M}_b^{(m)^{-1}}\boldsymbol{B}^{(m)} \in \mathbb{R}^{n_j \times n_j}$ is equivalent to defining $[\boldsymbol{E}^{(m)}]_{ii} = [h'(c_i)]^{-1}$ if $i \in \mathcal{I}_b$ and 0 otherwise. Adding together (i) (15) multiplied on the left by $\boldsymbol{A}^T$, (ii) (16) multiplied on left by $\boldsymbol{B}^T$ and

(iii) the third block equation of (14) gives, noting that $\boldsymbol{B}^{(m)^T}\boldsymbol{M}_b^{(m)^{-1}}\boldsymbol{h}_b^{(m+1)} = \boldsymbol{B}^{(m)^T}\boldsymbol{M}_b^{(m)^{-1}}\boldsymbol{B}^{(m)}\boldsymbol{h}^{(m+1)} = \boldsymbol{E}^{(m)}\boldsymbol{h}^{(m)}$,

$$\left(\boldsymbol{A}^T\boldsymbol{F}^{(m)^{-1}}\boldsymbol{A} + \boldsymbol{E}^{(m)}\right)\boldsymbol{h}^{(m+1)} = \boldsymbol{E}^{(m)}\left(\boldsymbol{\theta}^{(m)} + h_m + \boldsymbol{u}\right) + \boldsymbol{A}^T\boldsymbol{F}^{(m)^{-1}}\left(\boldsymbol{G}^{(m)}\boldsymbol{q}^{(m)} - \boldsymbol{a}\right) + \boldsymbol{\rho}_m^{(m)}. \tag{17}$$

The dimension of Eq. (17) remains the same whatever the number of active constraints because the selection matrix $\boldsymbol{B}^{(m)}$ embeds the required partial delivery elements in a matrix of appropriate dimension. Equations (15)-(17) form the recurrence relations which are the basis of the iterative ASM for the heads, pipe flows and nodal outflows of the system.

In fact, equations (15)-(17) bear a striking resemblance to the corresponding equations for the EMR method: the two equations which define the iteration of the EMR method are (15) exactly as it stands and (17) without the first term on the right. This observation forms the basis of an algorithmic measure which is described later.

THE ACTIVE SET METHOD ALGORITHM

The algorithm which follows implements the ASM which was developed above. The iteration is run until either (i) the relative difference between the norms of successive iterates is sufficiently small or (ii) too many iterations have been executed. The issue of stalled iterations is discussed below.

Let N be the index set of all the nodes with unknown-head. Three index sets $\mathcal{I}_b, \mathcal{I}_l, \mathcal{I}_u$ are defined (only) for the nodes at which the nominal demand is positive, $d_i > 0$: The first is $\mathcal{I}_b$, the set of indices i at which (i) the outflow is between zero and the nominal demand $0 < c_i < d_i$, or (ii) the outflow is zero $c_i = 0$ but the corresponding Lagrange multiplier is negative $\lambda_i < 0$, or (iii) the outflow is at the nominal demand $c_i = d_i$ and the corresponding Lagrange multiplier is negative $\mu_i < 0$. More precisely, $\mathcal{I}_b^{(m+1)} = \left\{i \in N |\, d_i > 0 \wedge \left(\left(c_i^{(m+1)} > 0 \wedge c_i^{(m+1)} < d_i\right) \vee \quad \left(c_i^{(m+1)} = 0 \wedge \lambda_i^{(m+1)} < 0\right) \vee \left(c_i^{(m+1)} = d_i \wedge \mu_i^{(m+1)} < 0\right)\right)\right\}$; The second is the set $\mathcal{I}_l$ of indices i at which (i) the outflow is negative $c_i < 0$ or (ii) the outflow is zero $c_i = 0$ and the corresponding Lagrange multiplier is non-negative $\lambda_i \geq 0$. More precisely, $\mathcal{I}_l^{(m+1)} = \left\{i \in N |\, d_i > 0 \wedge \left(c_i^{(m+1)} < 0 \vee \left(c_i^{(m+1)} = 0 \wedge \lambda_i^{(m+1)} \geq 0\right)\right)\right\}$. The third is the set $\mathcal{I}_u$ of indices i for the nodes at which (i) the outflow is greater than the nominal demand $c_i > d_i$ or (ii) the outflow is at the nominal demand $c_i = d_i$ and the corresponding Lagrange multiplier is non-negative $\mu_i \geq 0$. More precisely, $\mathcal{I}_u^{(m+1)} = \left\{i \in N |\, d_i > 0 \wedge \left(c_i^{(m+1)} > d_i \vee \left(c_i^{(m+1)} = d_i \wedge \mu_i^{(m+1)} \geq 0\right)\right)\right\}$.;

Initialization

Initial values of $\boldsymbol{h}^{(0)}$ the heads, $\boldsymbol{q}^{(0)}$ the pipe flows and $\boldsymbol{c}^{(0)}$, the nodal outflows, the Lagrange multipliers $\boldsymbol{\lambda}^{(0)}$ and $\boldsymbol{\mu}^{(0)}$, and the three index sets $\mathcal{I}_b, \mathcal{I}_l, \mathcal{I}_u$ are required. These are described below.

The iteration loop

Start loop: For $m = 0, 1, 2, \ldots$ repeat steps (a) to (j) until the stopping test is satisfied

(a) Let n_b denote the number of elements in $\mathcal{I}_b$. Compute the matrix $\boldsymbol{M}_b^{(m)} \in \mathbb{R}^{n_b \times n_b}$ by

$$\boldsymbol{M}_b^{(m)} \leftarrow \text{diag}\left\{h'(c_{i_1}), h'(c_{i_2}), \ldots, h'(c_{i_{n_b}})\right\}, i_k \in \mathcal{I}_b, 1 \leq k \leq n_b \tag{18}$$

and the matrix $\boldsymbol{E}^{(m)} \in \mathbb{R}^{n_j \times n_j}$ by $[\boldsymbol{E}^{(m)}]_{ii} = [h'(c_i)]^{-1}$ if $i \in \mathcal{I}_b$ and 0 otherwise.

(b) $\boldsymbol{\rho}_m^{(m)} \leftarrow -\boldsymbol{A}^T\boldsymbol{q}^{(m)} - \boldsymbol{c}^{(m)}$

(c) Solve (17) for heads $\boldsymbol{h}^{(m+1)}$

(d) Use (15) to update the pipe flows $\boldsymbol{q}^{(m+1)}$

(e) Use (16) to update the nodal outflows $c_i^{(m+1)}$ for which $i \in \mathcal{I}_b$.

(f) $\boldsymbol{\lambda}^{(m+1)} \leftarrow -\left(\boldsymbol{h}^{(m+1)} - h_m - \boldsymbol{u}\right)$

(g) $\boldsymbol{\mu}^{(m+1)} \leftarrow \boldsymbol{h}^{(m+1)} - h_s - \boldsymbol{u}$

(h) Update the index sets $\mathcal{I}_b, \mathcal{I}_l, \mathcal{I}_u$.

(i) $\boldsymbol{c}^{(m+1)} \leftarrow \max(\boldsymbol{c}^{(m+1)}, 0)$

(j) $\boldsymbol{c}^{(m+1)} \leftarrow \min(\boldsymbol{c}^{(m+1)}, \boldsymbol{d})$

Unlike the case of pure projection methods, it is unnecessary here to check the final nodal outflows and Lagrange multipliers to ensure that there are no nodes with $c = 0$ and $\lambda < 0$ or $c = d$ and $\mu < 0$ since in that case the KKT conditions for a minimum cannot have been met.

IMPLEMENTATION ISSUES

Certain issues surrounding the implementation of the ASM are now discussed.

It is worth noting that the inverse of the Heaviside POR is zero for $c \in [0, d]$ so that the content term for the nodes reduces to $(h_m + u)c$. So, in that case $C(\boldsymbol{q}, \boldsymbol{c})$ is not strictly convex. Even so, the equivalent, alternative formulation $C(\boldsymbol{q})$ satisfies the required conditions and that establishes the existence and uniqueness of the solution when that POR is used. However, the zero derivative of the Heaviside POR and its inverse makes it unsuitable for the ASM as described here.

POR Issues

The cubic POR, $c_3(h)$, of Fujiwara & Ganesharajah (1993) has zero derivatives at $z = 0$ and $z = 1$ and this means that the derivative of its inverse grows beyond limit as c approaches 0 or d, $\lim_{c\to 0+} h_3'(c) = \lim_{c\to d-} h_3'(c) = \infty$. Similarly, for the logistic sigmoidal POR, c_σ, $\lim_{z\to-\infty} c_\sigma'(z) = \lim_{z\to+\infty} c_\sigma'(z) = 0$ with the consequence that the derivative of its inverse grows beyond limit as c approaches the ends of the interval $[0, d]$, $\lim_{c\to 0+} h_\sigma'(c) = \lim_{c\to d-} h_\sigma'(c) = \infty$. In fact, the inverse itself and its derivative are both undefined at the two end-points of the interval, 0 and d. A similar situation occurs with the 2-side regularized Wagner consumption function: the inverse function has infinite derivative at the two end-points of the interval, 0 and d. Fig. 1, which shows the cubic, the 2-side regularized Wagner and logistic sigmoidal PORs and Fig. 2, which shows their inverses illustrate this point. A different problem exists with the unregularized Wagner POR, $c_w(z)$: its derivative is undefined at $z = 0$ and the derivative of its inverse POR, $h_w'(c)$, vanishes at $c = 0$. These properties of the PORs may cause the raw ASM to fail in some instances unless they are addressed. But the refinements that are needed to address them are quite simple and are now described.

Regularizing the M_b Matrix by Derivative Assignment when Moving From $\mathcal{I}_l$ to $\mathcal{I}_b$

Consider the case where the unregularized Wagner POR is used with the ASM. It is possible that a node that belongs in the set $\mathcal{I}_l$ with $c = 0$ and $\lambda > 0$ in one iteration has, in the next iteration, $c = 0$ and $\lambda < 0$. Such a node is then classified as being in the index set $\mathcal{I}_b$ and calculating $\boldsymbol{M}_b^{(m)}$ would require computing the derivative of the inverse POR at $c = 0$ for that node using (18). For the unregularized Wagner POR this derivative $h_w'(0) = 0$ and so the matrix $\boldsymbol{M}_b^{(m)}$ has no inverse and the computations in (16) and (17) fail. The zero derivative is a consequence of the fact that $\lim_{z\to 0+} c_w'(z) = \infty$. Recall that at the solution it is impossible for a node to have outflow $c = 0$, $\lambda < 0$ and at the same time to satisfy the KKT conditions. The computational failure just described can be avoided, for any POR where this occurs, by applying a slight perturbation to the system: simply assigning a small nonzero value (the value 1 was used in the tests reported in this paper) to the derivative of the inverse POR. This strategy, called "derivative assignment", has the effect of putting a small nonzero term in the corresponding diagonal element (which would otherwise be undefined) of the matrix $\boldsymbol{E}^{(m)}$ and could be considered as similar to a partial regularization use of Levenberg Marquardt damping to the system. Alternatively, it can be seen as a restarting of the iteration. Importantly, it does not affect the solution since it is impossible to have $c = 0$ and $\lambda < 0$ when the KKT conditions are met. Some examples using this technique are reported in a later section.

Interval Reduction

The difficulties associated with the cubic, the logistic sigmoidal and the 2-side regularized Wagner PORs can be easily handled by reducing the c-interval from $c/d \in [0, 1]$ to $c/d \in [\delta, 1 - \delta]$, small $\delta > 0$. To effect this

change requires only (i) modifying the definitions of the three index sets $\mathcal{I}_l, \mathcal{I}_b, \mathcal{I}_u$ and (ii) changing steps (i) and (j) of the algorithm to restrict the values of c to lie in the interval $[d\delta, d(1-\delta)]$. In the tests reported below the logistic sigmoidal and cubic PORs were successfully used on the eight case study networks with results that differed in infinity norm by no more than 10^{-6}, the same value as the stopping tolerance that was used to terminate the iterations. The value $\delta = 10^{-5}$ was used in those tests.

Initialization

Three starting schemes were investigated: one, S_b, that sets the initial outflow values at the center of the interval $[0, d]$, one, S_u, which sets them to the upper limit d and one, S_l, which sets them to the lower limit 0. The parameter values for these three starting schemes are shown in Table 3.

In all the tests on the eight case study networks (discussed later) the scheme, S_b which sets the initial outflows to $d/2$ most often resulted in fewer iterations. For example, one test was conducted in which the demand magnification factor for the eight case study networks was set at 1 (so as to make the problems almost DDM problems in which the delivery fractions for all networks were between 70 and 99%) and the two starting schemes S_b and S_u were compared. It might be thought that the starting scheme S_u would provide a better initialization for this case seeing that most of the nodes in the networks would be at, or close to, full delivery mode. However, the difference between the number of EMR iterations for the two starting schemes S_b and S_u was mostly zero, a few times 1 and on one occasion 4. Similarly, the difference between the number of ASM iterations for the two starting schemes S_b and S_u was mostly zero, once 1 and once 2. In other words, the methods seems to be rather insensitive to the starting values on these networks. Consequently, the schemes S_l and S_u were not further investigated. It is worth noting that the practice of using the extended period simulation solution at one time step as the starting values for the next time step saves computation time in many cases.

Stalled Iterations and Termination

Iterative schemes such as the ASM and the EMR method are typically stopped if either a stopping test based on the small size of the relative difference between successive iterates is satisfied or if too many iterations have been performed. It is sometimes the case that the prescribed stopping tolerance for the test based on successive iterates is set too small with the result that iterate differences reach a lower limit beyond which they never reduce regardless of however many more iterations are run. This phenomenon occurs when the updates to the iterates in the algorithm being used compute to something that is at floating point roundoff level for the computation engine being used. To avoid this phenomena the computation can be stopped by monitoring the slope of a line of best fit to the most recent iterate differences and triggering a stop condition if that slope is sufficiently small. For example, the codes used for the simulations reported in this study used the three most recent iterate differences and triggered a stop condition when the slope of the best fit line to those three differences was smaller than 10^{-5}. The experience of the authors is that the EMR method rarely exhibits this phenomena and the iterate differences regularly reduce to below any stopping tolerance which is larger than a modest multiple of machine epsilon. In some cases, though, the ASM does exhibit this phenomena for larger stopping tolerances. However, the similarity between the equations for the two methods, described earlier, allows a simple and effective method for dealing with this phenomena when it occurs with the ASM: using (15), dropping the second equation (16) and using (17) with the first term on the right omitted is equivalent to switching from the ASM to the EMR method. Seeing that this phenomena typically occurs when the stalled ASM solution is close to the required solution, the EMR method used in this context does not require line search. Thus, the switch from ASM to EMR in this setting is extremely simple and effective. None of the examples reported in this study required this switch but it is the experience of the authors that this strategy is necessary for some problems.

EXAMPLES

All the calculations reported in this paper were conducted using codes specially written for the package Matlab R2016b (Mathworks 2016) and which exploit the sparse matrix arithmetic facilities available in that package. Matlab implements arithmetic that conforms to the IEEE Double Precision Standard and so machine epsilon for all these calculations was 2.2×10^{-16}.

An example network

The network shown in Fig. 8 is now used to demonstrate the ASM. In this network (i) all pipes have length 500 m (ii) all diameters are 300 mm (iii) all roughnesses are 0.03 mm (iv) the demands at nodes 1,3,4 are 0.25 m^3/s and the demand at node 2 is 0.375 m^3/s (v) the source elevation is 20 m (vi) the minimum pressure head $h_m = 0$ m and the service pressure head is $h_s = 20$ m (vii) the POR used is the 1-side regularized Wagner. The iterations were run until the relative difference between successive head, flow, and outflow iterates differed in infinity norm by less than 10^{-6}. Throughout the computation all four nodes with unknown head were in the index set $\mathcal{I}_b$. It took the EMR method 8 outer iterations and 14 line search steps to satisfy the stopping test while the ASM took seven iterations to satisfy the corresponding stopping test. The four solution nodes were in partial delivery mode at steady state and delivered between 22 and 33% of the required demands. As a whole, the system produced a delivery fraction $\delta_f = 25\%$ of the required total demand. The heads and flows of the solutions by the two methods differed in infinity norm by less than 4×10^{-16} (consistent with the quadratic convergence behaviour that would be expected from the Newton method). No additional EMR steps were required in the application of the ASM.

The results in Table 4 summarize the convergence data for this example. Columns 2 to 4 show the relative differences between successive iterates

$$\delta_h^{(m+1)} = \frac{\left\| \boldsymbol{h}^{(m+1)} - \boldsymbol{h}^{(m)} \right\|_\infty}{\left\| \boldsymbol{h}^{(m+1)} \right\|_\infty}, \quad \delta_q^{(m+1)} = \frac{\left\| \boldsymbol{q}^{(m+1)} - \boldsymbol{q}^{(m)} \right\|_\infty}{\left\| \boldsymbol{q}^{(m+1)} \right\|_\infty}, \quad \delta_c^{(m+1)} = \frac{\left\| \boldsymbol{c}_b^{(m+1)} - \boldsymbol{c}_b^{(m)} \right\|_\infty}{\left\| \boldsymbol{c}_b^{(m+1)} \right\|_\infty}$$

and columns 5-7 show the norms of the energy residuals, $\boldsymbol{\rho}_e^{(m)}$, mass residuals, $\boldsymbol{\rho}_m^{(m)}$, and outflow residuals $\boldsymbol{\rho}_{c_b}^{(m)} = \boldsymbol{\theta}_b^{(m)} - \boldsymbol{h}_b^{(m)} + h_m + \boldsymbol{u}_b$. The quadratic convergence of the Newton method is clearly evidenced by the approximate doubling of the number of correct decimal digits as the iterates approach the solution (Isaacson & Keller 1966, 93).

Eight case study networks

The EMR and ASM were applied to the eight case study networks with between 934 and 19,647 pipes and between 848 and 17,971 nodes and which were discussed in Elhay et al. (2016). The convergence behaviours of the two methods on these networks were compared. In all cases (i) the given network nominal demands were magnified by a factor of 5 to ensure a genuine PDM problem, (ii) the 1-side regularized Wagner POR was used (iii) the same starting values, S_b, were used for both methods and (iv) the stopping tolerance for the infinity norms of the relative differences between successive iterates was set at 10^{-6}.

Define the quantities

$$\tau_h = -\log_{10} \left\| \boldsymbol{h}_{emr} - \boldsymbol{h}_{asm} \right\|_\infty \text{ and } \tau_q = -\log_{10} \left\| \boldsymbol{q}_{emr} - \boldsymbol{q}_{asm} \right\|_\infty \tag{19}$$

(essentially, the number of decimal digits of agreement between the heads and flows solutions of the two methods) and denote by n_a the number of ASM iterations required to satisfy the stopping test. Denote by n_{e_1} the number of outer iteration of the EMR method and by n_{e_2} the number of line search steps taken by the EMR method to satisfy the stopping test. The computational cost of a line search step in an EMR iteration is smaller than the cost of an EMR outer iteration. Therefore, the values of the ratios $\zeta = n_a/(n_{e_1} + \frac{1}{2} n_{e_2})$, expressed as percentages, were used to compare the computational costs of the two methods.

The results are summarized in Table 5. The following remarks can be made. The solutions for the ASM and EMR agree to between 6.8 and 11.3 decimal digits. This is consistent with an iteration stopping tolerance used of 10^{-6}. The ASM took between 34% and 70% of the number of iterations, as measured by ζ, of the EMR method to satisfy the stopping test: the EMR method took between 8 and 15 outer iterations and between 7 and 25 inner iterations over the 8 networks while the ASM took between 9 and 11 iterations. This represents a considerable computational saving. None of the ASM runs on these examples required additional EMR steps to satisfy the stopping test. Results very similar to these were obtained for the quadratic and linear PORs.

Table 6 shows the wall clock time comparison for the two methods as reported by the Matlab profiler. These times are indicative only since, while all care was taken to make the codes efficient, no serious effort was made to optimize the codes for execution times because it is well known that Matlab timings are not normally used for this type of comparison. This is because the built-in functions in Matlab are extremely fast while running the interpretive codes in the program scripts can be quite slow (as could be expected in a research and development

package). Nevertheless, the significantly faster run times (five times faster in some cases) point to a method that further testing could confirm as being more rapid than the EMR. This further testing is beyond the scope or intent of this paper.

To illustrate the necessity to use the derivative assignment technique, the ASM was applied to the eight case study networks with the POR modelled by the unregularized Wagner formula. When no derivative assignment was used networks N_3, N_4, N_6, N_7 and N_8 did not solve because of the zero derivative of the inverse POR at $c = 0$ but the ASM solved all eight networks when derivative assignment was used.

In addition, eight virtual control networks which are the equivalents of the eight case study networks were constructed along the lines suggested by Fig. 5 and EPANET 2.0 was then applied to these networks. The column in Table 5 headed n_E shows the number of iterations that were required by EPANET to solve the equivalent virtual control networks using the unregularized Wagner POR. The larger number of iterations taken by EPANET are no doubt due in part to the very much larger dimensions of the equivalent virtual control networks. Network N_5 remained unbalanced by EPANET after more than 500 iterations. But, while the greater number of iterations required by EPANET is a disadvantage, the convergence failure and the large number of virtual control devices which need to be added to the original network are far more serious disadvantages (see Table 1).

Early active set methods allowed only one constraint to be added or released at a time (Hager & Zhang 2006), sometimes resulting in very slow convergence. Later developments led to methods, like the one presented in this paper, that add or release many constraints at once. To illustrate this point the number of nodes in the three index sets $\mathcal{I}_l$, $\mathcal{I}_b$ and $\mathcal{I}_u$ were recorded at each of the nine iterations that were required to solve for the heads, pipe flows and nodal outflows of the case study networks N_1 and N_7 by the ASM. Table 7 shows the set counts for those calculations. For N_1, the starting scheme, S_b put all 474 nodes into the index set $\mathcal{I}_b$ and fully 425 of those nodes had moved by the end of the first iteration to set $\mathcal{I}_u$. That is to say, the state of 425 constraints had changed from inactive to active in one step. Iterations 2, 3 and 4 also show many nodes changing set membership but even so, the method appears to accommodate these rapid changes of state very robustly. This example and the data for N_7, also in Table 7, is typical of the behaviour observed in all the tests conducted for this paper.

CONCLUSIONS

A new, fast and robust method for determining the steady-state heads, pipe flows and nodal outflows of WDSs using PDM has been presented. The new procedure is a content-based active set method and has been convincingly shown to take fewer iterations than its best competitor, the EMR method, for PDM problems. The authors believe that exhaustive testing (which is beyond the scope or intent of this paper) will establish that the method is very much faster (maybe several times faster in terms of wall-clock time) than the EMR method. The method is attractive because (i) it does not, like the EMR method, require damping, (ii) it does not require the addition of virtual elements to the model and more importantly, (iii) it succeeds in some cases where the EMR and EPANET fail and (iv) the new formulation is well-suited to superlinear characteristics which are associated with good convergence. The new method has box constraints whereas the EMR method has linear constraints which require selective projection techniques and these are harder to deal with.

The ASM requires slight refinement when used with some PORs: in particular, unregularized Wagner POR, the 2-side regularized Wagner POR, the logistic sigmoidal POR and the cubic POR. The unregularized Wagner POR needs the derivative assignment technique described above and the cubic, logistic and 2-side regularized Wagner need the interval reduction technique, also described above. The linear, quadratic, 1-side regularized Wagner and any other PORs with non-zero derivatives at the minimum and service pressure head points can all be used with the ASM as it stands without refinement.

Eight virtual control networks which are equivalent to the eight case study networks previously considered in Elhay et al. (2016) were generated along the lines in Fig. 5. The huge increase in the number of degrees of freedom and control devices necessary in such models clearly established that the new technique is far preferable to this approach. Furthermore, when EPANET 2 was applied to these networks with the unregularized Wagner POR, EPANET failed to converge for one of the networks while the ASM correctly found the solution for that network in just eight iterations.

There are cases where an iterative method stalls, for example, where the stopping tolerance for that particular method is set too small. In the event that the ASM stalls close to a solution it is possible to easily switch to the EMR which can, in some cases, produce solutions with smaller residuals. Although this switch was not

required in any of the tests reported in this paper, it is remarkably easy to implement and typically does not require damping or line search.

The operation of the ASM was demonstrated on an illustrative network and then the method was convincingly shown to take fewer iterations than its main competitor, the EMR method, on eight real, or realistic, case study networks with up to about 20,000 pipes and 18,000 nodes.

APPENDIX

REDUCING THE DIMENSION OF THE SYSTEM TO BE SOLVED

This appendix describes the rearrangement of (13) that reduces it to (14). This significantly reduces the dimension of the non-linear system to be solved.

The n_j nodes in the system are reordered into three block columns: the first for the nodes at which the outflow is dependent on the pressure, the second for the nodes at which the outflow is zero because of insufficient pressure and the third for the nodes at which there is full supply because the pressure is higher than the specified service pressure head. The matrix $\boldsymbol{M}$ and the selection matrices $\boldsymbol{L}$ and $\boldsymbol{U}$ are reordered

$$\boldsymbol{M} = \begin{array}{c} \\ n_b \\ n_l \\ n_u \end{array} \begin{array}{c} \begin{array}{ccc} n_b & n_l & n_u \end{array} \\ \begin{pmatrix} \boldsymbol{M}_b & \boldsymbol{O} & \boldsymbol{O} \\ \boldsymbol{O} & \boldsymbol{O} & \boldsymbol{O} \\ \boldsymbol{O} & \boldsymbol{O} & \boldsymbol{O} \end{pmatrix} \end{array}, \quad \boldsymbol{L} = \begin{array}{c} \\ n_l \end{array} \begin{array}{c} \begin{array}{ccc} n_b & n_l & n_u \end{array} \\ \begin{pmatrix} \boldsymbol{O} & \boldsymbol{I}_{n_l} & \boldsymbol{O} \end{pmatrix} \end{array}, \quad \boldsymbol{U} = \begin{array}{c} \\ n_u \end{array} \begin{array}{c} \begin{array}{ccc} n_b & n_l & n_u \end{array} \\ \begin{pmatrix} \boldsymbol{O} & \boldsymbol{O} & \boldsymbol{I}_{n_u} \end{pmatrix} \end{array}.$$

The system (13) is, with the obvious reordering of the columns of $\boldsymbol{A}$, now

$$\begin{array}{c} \\ n_p \\ n_a \\ n_l \\ n_u \\ n_b \\ n_l \\ n_u \\ n_l \\ n_u \end{array} \begin{array}{c} \begin{array}{ccccccccc} n_p & n_b & n_l & n_u & n_b & n_l & n_u & n_l & n_u \end{array} \\ \begin{pmatrix} \boldsymbol{F}^{(m)} & \boldsymbol{O} & \boldsymbol{O} & \boldsymbol{O} & -\boldsymbol{A}_b & -\boldsymbol{A}_l & -\boldsymbol{A}_u & \boldsymbol{O} & \boldsymbol{O} \\ \boldsymbol{O} & \boldsymbol{M}_b^{(m)} & \boldsymbol{O} & \boldsymbol{O} & -\boldsymbol{I} & \boldsymbol{O} & \boldsymbol{O} & \boldsymbol{O} & \boldsymbol{O} \\ \boldsymbol{O} & \boldsymbol{O} & \boldsymbol{O} & \boldsymbol{O} & \boldsymbol{O} & -\boldsymbol{I} & \boldsymbol{O} & -\boldsymbol{I} & \boldsymbol{O} \\ \boldsymbol{O} & \boldsymbol{O} & \boldsymbol{O} & \boldsymbol{O} & \boldsymbol{O} & \boldsymbol{O} & -\boldsymbol{I} & \boldsymbol{O} & \boldsymbol{I} \\ -\boldsymbol{A}_b^T & -\boldsymbol{I} & \boldsymbol{O} & \boldsymbol{O} & \boldsymbol{O} & \boldsymbol{O} & \boldsymbol{O} & \boldsymbol{O} & \boldsymbol{O} \\ -\boldsymbol{A}_l^T & \boldsymbol{O} & -\boldsymbol{I} & \boldsymbol{O} & \boldsymbol{O} & \boldsymbol{O} & \boldsymbol{O} & \boldsymbol{O} & \boldsymbol{O} \\ -\boldsymbol{A}_u^T & \boldsymbol{O} & \boldsymbol{O} & -\boldsymbol{I} & \boldsymbol{O} & \boldsymbol{O} & \boldsymbol{O} & \boldsymbol{O} & \boldsymbol{O} \\ \boldsymbol{O} & \boldsymbol{O} & -\boldsymbol{I} & \boldsymbol{O} & \boldsymbol{O} & \boldsymbol{O} & \boldsymbol{O} & \boldsymbol{O} & \boldsymbol{O} \\ \boldsymbol{O} & \boldsymbol{O} & \boldsymbol{O} & \boldsymbol{I} & \boldsymbol{O} & \boldsymbol{O} & \boldsymbol{O} & \boldsymbol{O} & \boldsymbol{O} \end{pmatrix} \end{array} \begin{pmatrix} \boldsymbol{q}^{(m+1)} - \boldsymbol{q}^{(m)} \\ \boldsymbol{c}_b^{(m+1)} - \boldsymbol{c}_b^{(m)} \\ \boldsymbol{c}_l^{(m+1)} - \boldsymbol{c}_l^{(m)} \\ \boldsymbol{c}_u^{(m+1)} - \boldsymbol{c}_u^{(m)} \\ \boldsymbol{h}_b^{(m+1)} - \boldsymbol{h}_b^{(m)} \\ \boldsymbol{h}_l^{(m+1)} - \boldsymbol{h}_l^{(m)} \\ \boldsymbol{h}_u^{(m+1)} - \boldsymbol{h}_u^{(m)} \\ \boldsymbol{\lambda}^{*(m+1)} - \boldsymbol{\lambda}^{*(m)} \\ \boldsymbol{\mu}^{*(m+1)} - \boldsymbol{\mu}^{*(m)} \end{pmatrix} = - \begin{pmatrix} \boldsymbol{\rho}_e^{(m)} \\ \boldsymbol{\theta}_b^{(m)} + h_m - \boldsymbol{h}_b^{(m)} + \boldsymbol{u}_b \\ h_m - \boldsymbol{h}_l^{(m)} + \boldsymbol{u}_l - \boldsymbol{\lambda}^{*(m)} \\ h_s - \boldsymbol{h}_u{}^{(m)} + \boldsymbol{u}_u + \boldsymbol{\mu}^{*(m)} \\ -\boldsymbol{A}_b^T \boldsymbol{q}^{(m)} - \boldsymbol{c}_b^{(m)} \\ -\boldsymbol{A}_l^T \boldsymbol{q}^{(m)} - \boldsymbol{c}_l^{(m)} \\ -\boldsymbol{A}_u^T \boldsymbol{q}^{(m)} - \boldsymbol{c}_u^{(m)} \\ \boldsymbol{c}_l^{(m)} \\ \boldsymbol{c}_u^{(m)} - \boldsymbol{U}^{(m)} \boldsymbol{d} \end{pmatrix} \tag{20}$$

The last two block equations assert that the outflows at nodes with insufficient pressure are zero, $\boldsymbol{c}_l^{(m+1)} = \boldsymbol{o}$, and that the outflows at nodes with pressure higher than the service pressure head are the full, nominal demands, $\boldsymbol{c}_u^{(m+1)} = \boldsymbol{U}^{(m)} \boldsymbol{d}$. Thus, (i) block columns 3 and 4 and block rows 8 and 9 of the system matrix, (ii) block rows 3 and 4 of the vector on the left can be dropped and (iii) block rows 8 and 9 of the vector on the right of the system can therefore be dropped to give the reduced system

$$
\begin{array}{c} \\ n_p \\ n_a \\ n_l \\ n_u \\ n_b \\ n_l \\ n_u \end{array}
\begin{array}{c}
\begin{array}{ccccccc} n_p & n_b & n_b & n_l & n_u & n_l & n_u \end{array} \\
\begin{pmatrix}
\boldsymbol{F}^{(m)} & \boldsymbol{O} & -\boldsymbol{A}_b & -\boldsymbol{A}_l & -\boldsymbol{A}_u & \boldsymbol{O} & \boldsymbol{O} \\
\boldsymbol{O} & \boldsymbol{M}_b^{(m)} & -\boldsymbol{I} & \boldsymbol{O} & \boldsymbol{O} & \boldsymbol{O} & \boldsymbol{O} \\
\boldsymbol{O} & \boldsymbol{O} & \boldsymbol{O} & -\boldsymbol{I} & \boldsymbol{O} & -\boldsymbol{I} & \boldsymbol{O} \\
\boldsymbol{O} & \boldsymbol{O} & \boldsymbol{O} & \boldsymbol{O} & -\boldsymbol{I} & \boldsymbol{O} & \boldsymbol{I} \\
-\boldsymbol{A}_b^T & -\boldsymbol{I} & \boldsymbol{O} & \boldsymbol{O} & \boldsymbol{O} & \boldsymbol{O} & \boldsymbol{O} \\
-\boldsymbol{A}_l^T & \boldsymbol{O} & \boldsymbol{O} & \boldsymbol{O} & \boldsymbol{O} & \boldsymbol{O} & \boldsymbol{O} \\
-\boldsymbol{A}_u^T & \boldsymbol{O} & \boldsymbol{O} & \boldsymbol{O} & \boldsymbol{O} & \boldsymbol{O} & \boldsymbol{O}
\end{pmatrix}
\end{array}
\begin{pmatrix}
\boldsymbol{q}^{(m+1)} - \boldsymbol{q}^{(m)} \\
\boldsymbol{c}_b^{(m+1)} - \boldsymbol{c}_b^{(m)} \\
\boldsymbol{h}_b^{(m+1)} - \boldsymbol{h}_b^{(m)} \\
\boldsymbol{h}_l^{(m+1)} - \boldsymbol{h}_l^{(m)} \\
\boldsymbol{h}_u^{(m+1)} - \boldsymbol{h}_u^{(m)} \\
\boldsymbol{\lambda}^{*(m+1)} - \boldsymbol{\lambda}^{*(m)} \\
\boldsymbol{\mu}^{*(m+1)} - \boldsymbol{\mu}^{*(m)}
\end{pmatrix} =
$$

$$
- \begin{pmatrix}
\boldsymbol{\rho}_e^{(m)} \\
\boldsymbol{\theta}_b^{(m)} - \boldsymbol{h}_b^{(m)} + h_m + \boldsymbol{u}_b \\
-\boldsymbol{h}_l^{(m)} + h_m + \boldsymbol{u}_l - \boldsymbol{\lambda}^{*(m)} \\
-\boldsymbol{h}_u{}^{(m)} + h_s + \boldsymbol{u}_u + \boldsymbol{\mu}^{*(m)} \\
-\boldsymbol{A}_b^T \boldsymbol{q}^{(m)} - \boldsymbol{c}_b^{(m)} \\
-\boldsymbol{A}_l^T \boldsymbol{q}^{(m)} \\
-\boldsymbol{A}_u^T \boldsymbol{q}^{(m)} - \boldsymbol{U}^{(m)} \boldsymbol{d}
\end{pmatrix}. \tag{21}
$$

Similarly, the third block equation in (21) gives the relation $\boldsymbol{\lambda}^{*(m+1)} = h_m + \boldsymbol{u}_l - \boldsymbol{h}_l^{(m+1)}$ and the fourth block equation in (21) gives $\boldsymbol{\mu}^{*(m+1)} = \boldsymbol{h}_u^{(m+1)} - \boldsymbol{u}_u - h_s$ which allows (i) block rows 3 and 4 and block columns 6 and 7 of the matrix in (21) to be dropped, (ii) block rows 6 and 7 of the vector on the left and (iii) block rows 3 and 4 of the vector on the right to be dropped. The resulting system is

$$
\begin{array}{c} \\ n_p \\ n_a \\ n_b \\ n_l \\ n_u \end{array}
\begin{array}{c}
\begin{array}{ccccc} n_p & n_b & n_b & n_l & n_u \end{array} \\
\begin{pmatrix}
\boldsymbol{F}^{(m)} & \boldsymbol{O} & -\boldsymbol{A}_b & -\boldsymbol{A}_l & -\boldsymbol{A}_u \\
\boldsymbol{O} & \boldsymbol{M}_b^{(m)} & -\boldsymbol{I} & \boldsymbol{O} & \boldsymbol{O} \\
-\boldsymbol{A}_b^T & -\boldsymbol{I} & \boldsymbol{O} & \boldsymbol{O} & \boldsymbol{O} \\
-\boldsymbol{A}_l^T & \boldsymbol{O} & \boldsymbol{O} & \boldsymbol{O} & \boldsymbol{O} \\
-\boldsymbol{A}_u^T & \boldsymbol{O} & \boldsymbol{O} & \boldsymbol{O} & \boldsymbol{O}
\end{pmatrix}
\end{array}
\begin{pmatrix}
\boldsymbol{q}^{(m+1)} - \boldsymbol{q}^{(m)} \\
\boldsymbol{c}_b^{(m+1)} - \boldsymbol{c}_b^{(m)} \\
\boldsymbol{h}_b^{(m+1)} - \boldsymbol{h}_b^{(m)} \\
\boldsymbol{h}_l^{(m+1)} - \boldsymbol{h}_l^{(m)} \\
\boldsymbol{h}_u^{(m+1)} - \boldsymbol{h}_u^{(m)}
\end{pmatrix} = -
\begin{pmatrix}
\boldsymbol{\rho}_e^{(m)} \\
\boldsymbol{\theta}_b^{(m)} - \boldsymbol{h}_b^{(m)} + h_m + \boldsymbol{u}_b \\
-\boldsymbol{A}_b^T \boldsymbol{q}^{(m)} - \boldsymbol{c}_b^{(m)} \\
-\boldsymbol{A}_l^T \boldsymbol{q}^{(m)} \\
-\boldsymbol{A}_u^T \boldsymbol{q}^{(m)} - \boldsymbol{U}^{(m)} \boldsymbol{d}
\end{pmatrix}. \tag{22}
$$

If the selection matrix $\boldsymbol{B}^{(m)}$ is defined by $\boldsymbol{B}^{(m)} = \begin{array}{c} \\ n_b \end{array} \begin{array}{c} \begin{array}{ccc} n_b & n_l & n_u \end{array} \\ \begin{pmatrix} \boldsymbol{I} & \boldsymbol{O} & \boldsymbol{O} \end{pmatrix} \end{array}$, then (22) can be written more compactly as (14).

POR MODELS, INVERSES AND DERIVATIVES

The general form of a POR, $c(h)$, was defined in (2) and the general form of the inverse POR was defined in (3). In this appendix are listed, for the interval $0 < z(h) < 1$, the functional forms of particular PORs and their derivatives. Also listed are the functional forms, for the interval $0 < c < d$, of the corresponding inverse POR functions and their derivatives. Only those PORs which have been used in this study are presented.

The linear POR is $c_1(h) = d\,z(h)$ and its derivative is $c_1'(h) = d/(h_s - h_m)$. The inverse is $h_1(c) = h_m + u + (h_s - h_m)(c/d)$ and its derivative is $h_1'(c) = (h_s - h_m)/d$.

A quadratic POR which loosely follows the Wagner function but which, unlike the Wagner POR, has a finite derivative at $z = 0$ is introduced. With z as in (1) this POR is defined by $c_2(h) = \frac{d}{4} z(h)(7 - 3z(h))$ and its derivative is $c_2'(h) = \frac{d}{4}(7 - 6z(h))/(h_s - h_m)$. The inverse POR is $h_2(c) = h_m + u + \frac{1}{6}(h_s - h_m)\left(7 - \sqrt{49 - 48(c/d)}\right)$ and its derivative is $h_2'(c) = 4(h_s - h_m)/\left(d\sqrt{49 - 48(c/d)}\right)$ In fact, $\max_{z\in[0,1]} |c_2(z) - c_w(z)| < 0.15$. This POR has the properties $c_2(0) = 0$, $c_2'(0) = 7d/(4(h_s - h_m))$, $c_2(1) = d$ and, importantly for the ASM method, the derivative of the inverse at $c = d$ is not infinite, $h_2'(d) = 1/c_2'(1) = 4(h_s - h_m)/d$. Fig. 4 shows the POR $c_2(z)$ and the unregularized Wagner POR, $c_w(z)$, together.

The (Unregularized) Wagner POR (Wagner et al. 1988) is defined by $c_w(h) = d\sqrt{z(h)}$. Its derivative is $c_w'(h) = d/\left(2(h_s - h_m)\sqrt{z(h)}\right)$ and so the inverse POR is $h_w(c) = h_m + u + (h_s - h_m)\,(c/d)^2$. The derivative of the inverse POR is $h_w'(c) = 2(h_s - h_m)\,(c/d^2)$.

The new, **1-side regularized Wagner** POR, $c_s(z)$, is derived from the Wagner POR by replacing the original square root function by a quadratic on the interval $[0, \epsilon]$, $\epsilon > 0$ some small number. The quadratic is chosen to agree with the Wagner POR and it's derivative at the point ϵ, and to have a finite derivative at $z = 0$. It therefore has the following properties $c_s(0) = 0$, $c_s(\epsilon) = d\sqrt{\epsilon}$, $c_s'(\epsilon) = d/(2(h_s - h_m)\sqrt{\epsilon})$ making it C^0 on $z \in [0, 1]$.

This POR is defined, on $z \in [0, \epsilon]$, by the quadratic $c_s(h) = dz(3\epsilon - z)/\,(2\epsilon\sqrt{\epsilon})$. Its derivative on the same interval is $c_s'(h) = d(3\epsilon - 2z)/\,(2\epsilon\sqrt{\epsilon}(h_s - h_m))$. Its inverse on $[0, d\sqrt{\epsilon}]$ is given by $h_s(c) = h_m + u + (h_s - h_m)\left(\frac{3\epsilon}{2} - \frac{1}{2}\sqrt{9\epsilon^2 - 8\epsilon\sqrt{\epsilon}\left(\frac{c}{d}\right)}\right)$

and its derivative on that same interval is given by $h_s'(c) = 2(h_s - h_m)\epsilon\sqrt{\epsilon}/\left(d\sqrt{9\epsilon^2 - 8\epsilon\sqrt{\epsilon}\left(\frac{c}{d}\right)}\right)$. This POR, its inverse and their derivatives exactly match the unregularized Wagner POR on the complementary intervals. Fig. 3 shows the one-side regularized Wagner POR, $c_s(h)$, and its inverse. The solid line represents the quadratic component of the POR and the dashed line represents the original Wagner component.

For $0 < z < 1$, **the Heaviside POR** (Bhave 1981, Piller & Van Zyl 2007) is defined by $c_h(h) = d$ and its derivative $c'(h) = 0$ for all h. Its inverse is given by $h_h(c) = h_m + u$ and the derivative of its inverse is zero, $h_h'(c) = 0$ for all $0 < c < d$.

The logistic, sigmoidal or exponential POR of (Tanyimboh & Templeman 2004) is given, with z as in (1), by $c_\sigma(h) = d\frac{e^{\alpha+\beta z}}{1+e^{\alpha+\beta z}}$. It is based on the inverse of the logit function, $\text{logit}(x) = \ln(x/(1-x))$, since $\text{logit}^{-1}(x) = 1/(1+e^{-x})$. In the absence of empirical data by which to determine the parameters α, β, they can be assigned values by choosing a small parameter δ and then using $\alpha = \text{logit}(\delta)$ and $\beta = -2\alpha$. The h-derivative of the logistic sigmoidal POR on the interval $0 < z < 1$ is given by $c_\sigma'(h) = d\frac{\beta}{h_s - h_m}\frac{e^{\alpha+\beta z}}{(1+e^{\alpha+\beta z})^2}$ and the inverse POR for $0 < c < d$ is given by $h_\sigma(c) = h_m + u + \frac{h_s - h_m}{\beta}\left(\ln\left(\frac{c}{d-c}\right) - \alpha\right)$. Finally, the derivative of the inverse is given by $h_\sigma'(c) = \frac{(h_s - h_m)}{\beta}\frac{1}{c(1-c/d)}$.

The inverse logistic function can also be expressed in terms of the quantile function for the logistic distribution (Gilchrist 2000): the inverse logistic is the quantile function $Q(p; \mu, s)$ with $p = c/d$, $s = (h_m - h_s)/\beta$ and $\mu = h_m + u - \frac{\alpha}{\beta}/(h_s - h_m)$. Thus, $\mu = h_m + u + (h_s - h_m)/2 = (h_s + h_m)/2 + u$. Then, $Q'(p; s) = s/(p(1-p))$ and so $h_\sigma'(c) = Q'(p; s)\frac{1}{d}$.

ACKNOWLEDGMENTS

The work presented in this paper is part of the French-German collaborative research project ResiWater that is funded by the French National Research Agency (ANR; project: ANR-14-PICS-0003) and the German Federal Ministry of Education and Research (BMBF; project: BMBF-13N13690). The authors gratefully acknowledge the anonymous reviewers whose comments led to an improved paper.

SUPPLEMENTAL DATA

The EPANET `.inp` files for the network shown in Fig. 8, networks N_1, N_3, N_4 and N_7 (which are listed in Table 1) and their virtual control equivalent networks are available online in the ASCE Library (www.ascelibrary.org). The other four networks N_2, N_5, N_6 and N_8 are not freely available either because they are proprietary or because of security concerns.

References

Bhave, P. R. (1981), 'Node flow analysis distribution systems', *Transportation Engineering Journal* **107**(4), 457–467.

Ciaponi, C., Franchioli, L., Murari, E. & Papiri, S. (2015), 'Procedure for defining a pressure-outflow relationship regarding indoor demands in pressure-driven analysis of water distribution networks', *Water Resour. Manage.* **29**, 817–832. DOI: 10.1007/s11269-014-0845-2.

Cramer, J. (2003), *Logit Models From Economics and Other Fields*, Cambridge University Press, Cambridge.

Deuerlein, J. W. (2002), On the hydraulic system analysis of water supply networks (in German), PhD thesis, Department of Civil Engineering, Geo- and Environmental Sciences, University of Karlsruhe (TH). Germany.

Elhay, S., Piller, O., Deuerlein, J. W. & Simpson, A. R. (2016), 'A robust, rapidly convergent method that solves the water distribution equations for pressure dependent models', *J. Water Resour. Plann. Manage.* **142**(2). DOI: 10.1061/(ASCE)WR.1943-5452.0000578.

Fujiwara, O. & Ganesharajah, T. (1993), 'Reliability assessment of water supply systems with storage and distribution networks', *Water Resour. Res* **29**(8), 2917–2924.

Germanopoulos, G. (1985), 'A technical note on the inclusion of pressure dependent demand and leakage terms in water supply network models', *Civ. Eng. Syst.* **2**(3), 171–179.

Gilchrist, W. (2000), *Statistical Modelling with Quantile Functions*, Chapman & Hall/CRC, London.

Giustolisi, O., Savic, D. & Kapelan, Z. (2008), 'Pressure-driven demand and leakage simulation for water distribution networks', *J. Hydraul. Eng.* **134**(5), 626–635.

Goldstein, A. (1967), *Constructive Real Analysis*, Dover Publications, Mineola, New York.

Gupta, R. & Bhave, P. (1996), 'Comparison of methods for predicting deficient network performance', *Water Resour. Manage.* **122**(3), 214–217.

Hager, W. & Zhang, H. (2006), 'A new active set method for box constrained optimization', *SIAM J. Optim.* **17**(2), 526–557.

Isaacson, E. & Keller, H. (1966), *Analysis of numerical methods*, Wiley, New York.

Jun, L. & Guoping, Y. (2013), 'Iterative methodology of pressure-dependent demand based on EPANET for pressure-deficient water distribution analysis', *J. Water Resour. Plann. Manage.* **139**(1), 34–44. DOI: 10.1061/(ASCE)WR.1943-5452.0000227.

Lippai, I. & Wright, L. (2014), 'Demand constructs for risk analysis', *Procedia Engineering* **89**, 640–647. 16th Water Distribution System Analysis Conference, WDSA2014 Urban Water Hydroinformatics and Strategic Planning.

Mahmoud, H., Savic, D. & Kapelan, Z. (2017), 'New pressure-driven approach for modeling water distribution networks', *J. Water. Resour. Plann. Manage.* **143**(8), 4017031. DOI: 10.1061/(ASCE)WR.1943-5452.0000781.

Mathworks, T. (2016), *MATLAB version 9.1.0.441655 (R2016b)*, Natick, Massachusetts.

Piller, O., Bremond, B. & Poulton, M. (2003), Least action principles appropriate to pressure driven models of pipe networks, *in* 'World Water & Environmental Resources Congress 2003', ASCE, pp. 1–15. DOI: 10.1061/40685(2003)113.

Piller, O., Elhay, S., Deuerlein, J. W. & Simpson, A. R. (2017), Why are line search methods needed for hysdraulic ddm and pdm solvers, *in* R. Collins, ed., 'Computing and Control for the Water Industry 2017', Research Studies Press ltd. DOI: 10.15131/shef.data.c.3867985.v1.

Piller, O. & Van Zyl, J. (2007), A unified framework for pressure driven network analysis, *in* 'Proc. of Computer and Control in Water Industry, Water Management Challenges in Global Changes, Supplementary Proceedings', Taylor & Francis, London, pp. 25–30.

ResiWater (2018), 'Resiwater: Innovative secure sensor networks and model-based assessment tools for increased resilience of water infrastructures'. `http://www.resiwater.eu/project/`.

Rossman, L. (2000), *EPANET 2 Users Manual*, Water Supply and Water Resources Division, National Risk Management Research Laboratory, Cincinnati, OH45268.

Shirzad, A., Tabesh, M., Farmani, R. & Mohammadi, M. (2013), 'Pressure-discharge relations with application in head driven simulation of water distribution networks', *J. Water. Resour. Plann. Manage.* **139**(6), 660–670. DOI: 10.1061/(ASCE)WR.1943-5452.0000305.

Siew, C. & Tanyimboh, T. (2012), 'Pressure-dependent EPANET extension', *Water Resour Manage* **26**, 1477–1498. DOI: 10.1007/s11269-011-9968-x.

Tanyimboh, T. & Templeman, A. (2004), A new nodal outflow function for water distribution networks, *in* C. Topping & M. Soares, eds, 'Proceedings of the Fourth International Conference on Engineering Computational Technology', number Paper 64 *in* 'B.H.V.', Civil-Comp Press, Stirlingshire, UK. DOI: 10.4203/ccp.80.64.

Todini, E. & Rossman, L. (2013), 'Unified framework for deriving simultaneous equation algorithms for water distribution networks.', *J. Hydraul. Eng.* **139**(5), 511–526.

Wagner, J., Shamir, U. & Marks, D. (1988), 'Water distribution reliability: simulation methods', *J. Water Resour. Plann. Manage.* **114**(3), 276–294. DOI: 10.1061/(ASCE)0733-9496(1988)114:3(276).

Table 1: Table showing the basic network statistics for the eight original case study networks and the statistics for the corresponding virtual control device equivalent network.

ID	n_p	n_j	n_f	$n_p^v + n_c^v$	n_j^v	n_f^v	$\frac{(n_p^v+n_c^v)}{n_p}$	n_j^v/n_j	n_f^v/n_f
N_1	934	848	8	2356	1796	482	2.52	2.12	60.25
N_2	1118	1039	2	3101	2361	663	2.77	2.27	331.50
N_3	1976	1770	4	7286	5310	1774	3.69	3.00	443.50
N_4	2465	1890	3	7292	5108	1612	2.96	2.70	537.33
N_5	2508	2443	2	6231	4925	1243	2.48	2.02	621.50
N_6	8584	8392	2	18103	14738	3175	2.11	1.76	1587.50
N_7	14830	12523	7	46486	33627	10559	3.13	2.69	1508.43
N_8	19647	17971	15	65643	48635	15347	3.34	2.71	1023.13

Note: The last three columns show the ratios of the link, node and source numbers.

Table 2: Formulae for functional form in terms of the head fraction, z on $0 \leq z \leq 1$ for various PORs discussed in this paper.

POR	Reference	$\gamma(z)$
Linear	Elhay et al. (2016)	z
Quadratic	The present study	$\frac{z}{4}(7-3z)$
Cubic	Fujiwara & Ganesharajah (1993)	$z^2(3-2z)$
Unregularized Wagner	Wagner et al. (1988)	$\sqrt{z}$
1-side Regularized Wagner	The present study	$\begin{cases} \frac{z(3\epsilon-z)}{2\epsilon\sqrt{\epsilon}} & \text{if } z < \epsilon \\ \sqrt{z} & \text{if } z \geq \epsilon \end{cases}$
2-side Regularized Wagner	Piller et al. (2003)	See Piller et al. (2003)
Logistic Sigmoidal	Tanyimboh & Templeman (2004)	$\frac{e^{\alpha+\beta z}}{1+e^{\alpha+\beta z}}$
Heaviside	Piller & Van Zyl (2007)	$\begin{cases} 0 & \text{if } z < 0 \\ 1 & \text{if } z \geq 0 \end{cases}$

Table 3: The values of various parameters for the three starting schemes S_l, S_b and S_u, which were used.

Parameter	S_l	S_b	S_u
$\boldsymbol{v}^{(0)}$ (m/s)	1/3	1/3	1/3
$\boldsymbol{c}^{(0)}$ (L/s)	$\boldsymbol{o}$	$\frac{1}{2}\boldsymbol{d}$	$\boldsymbol{d}$
$\boldsymbol{h}^{(0)}$ (m)	$h_m + \boldsymbol{u} - 1$	$\boldsymbol{h}(\boldsymbol{c}^{(0)})$	$h_s + \boldsymbol{u} + 1$
$\boldsymbol{\lambda}^{(0)}$ (m)	1	$-\left(\boldsymbol{h}^{(0)} - h_m - \boldsymbol{u}\right)$	$-(h_s - h_m) - 1$
$\boldsymbol{\mu}^{(0)}$ (m)	$-(h_s - h_m) - 1$	$\boldsymbol{h}^{(0)} - h_s - \boldsymbol{u}$	1
$\mathcal{I}_l^{(0)}$	$\{i \in N \vert d_i > 0\}$	$\emptyset$	$\emptyset$
$\mathcal{I}_b^{(0)}$	$\emptyset$	$\{i \in N \vert d_i > 0\}$	$\emptyset$
$\mathcal{I}_u^{(0)}$	$\emptyset$	$\emptyset$	$\{i \in N \vert d_i > 0\}$

Note: The initial flows are derived from an initial fluid velocity, $\boldsymbol{v}^{(0)}$, of 1/3 m/s.

Table 4: The convergence data for the ASM applied to the illustrative network shown in Fig. 8

m	$\delta_h^{(m)}$	$\delta_q^{(m)}$	$\delta_{c_b}^{(m)}$	$\left\Vert\boldsymbol{\rho}_e^{(m)}\right\Vert_\infty$	$\left\Vert\boldsymbol{\rho}_m^{(m)}\right\Vert_\infty$	$\left\Vert\boldsymbol{\rho}_{c_b}^{(m)}\right\Vert_\infty$
1	$9.68\,10^{-01}$	$5.06\,10^{-01}$	$2.74\,10^{-01}$	$5.46\,10^{+00}$	$7.40\,10^{-16}$	$1.31\,10^{+00}$
2	$7.67\,10^{-01}$	$3.68\,10^{+00}$	$7.99\,10^{-01}$	$1.07\,10^{+00}$	$1.48\,10^{-16}$	$1.88\,10^{+00}$
3	$3.91\,10^{-01}$	$4.28\,10^{-02}$	$4.29\,10^{-01}$	$1.45\,10^{-01}$	$1.85\,10^{-16}$	$2.33\,10^{-01}$
4	$7.83\,10^{-02}$	$9.06\,10^{-03}$	$9.36\,10^{-02}$	$5.00\,10^{-03}$	$1.11\,10^{-16}$	$9.06\,10^{-03}$
5	$2.94\,10^{-03}$	$5.62\,10^{-04}$	$4.16\,10^{-03}$	$7.00\,10^{-06}$	$1.48\,10^{-16}$	$1.68\,10^{-05}$
6	$4.24\,10^{-06}$	$2.42\,10^{-06}$	$8.59\,10^{-06}$	$1.46\,10^{-11}$	$7.40\,10^{-17}$	$7.16\,10^{-11}$
7	$1.58\,10^{-11}$	$1.92\,10^{-11}$	$3.95\,10^{-11}$	$1.39\,10^{-18}$	$1.30\,10^{-16}$	$4.44\,10^{-16}$

Note: see the section entitled "An Example Network" for the column heading definitions.

Table 5: Network characteristics and comparison of the performance of the ASM and the EMR methods applied to eight case study networks each with a demand magnification factor $f_{mag} = 5$. The numbers $n_\times$ with $\times = a, e, E$ designate iteration counts for the ASM, EMR and EPANET methods, respectively.

ID	n_p	n_j	n_f	n_{e_1}	n_{e_2}	$^{n_{e_1}+}_{n_{e_2}}$	n_a	n_E	τ_q	τ_h	$\delta_f\%$	$\zeta\%$
N_1	934	848	8	9	9	18	9	14	6.8	7.1	89.0	67
N_2	1118	1039	2	9	8	17	9	21	7.7	10.6	65.6	69
N_3	1976	1770	4	14	25	39	9	16	9.8	10.9	93.9	34
N_4	2465	1890	3	15	25	40	11	20	11.3	10.2	27.4	40
N_5	2508	2443	2	8	7	15	8	510*	8.2	9.7	51.3	70
N_6	8584	8392	2	8	7	15	8	31	8.7	9.5	70.6	70
N_7	14830	12523	7	10	13	23	9	15	9.7	10.2	59.6	55
N_8	19647	17971	15	10	9	19	10	41	9.4	10.4	97.7	69

* EPANET 2 "solution unbalanced after 510 trials" (iterations). See Eq. (19) for the definitions of τ_h, and τ_q. The delivery fractions are shown by δ_f and ζ shows the savings as defined in the text.

Table 6: Indicative wall clock times for the ASM and EMR runs on the eight case study networks as reported by the Matlab profiler.

Net	ASM (s)	EMR (s)	$\frac{ASM}{EMR}\%$
N_1	0.150	0.250	60
N_2	0.150	0.250	60
N_3	0.190	0.730	26
N_4	0.240	0.900	27
N_5	0.200	0.400	50
N_6	0.440	1.950	23
N_7	1.380	8.248	17
N_8	1.798	10.150	18

Note: While all care was taken to make the codes efficient, no serious effort was made at optimization of code execution for the reasons given in the text.

Table 7: The counts of the number of members in each of the three sets $\mathcal{I}_l$, $\mathcal{I}_b$ and $\mathcal{I}_u$ in each of the nine iterations required to solve the networks N_1 and N_7 by the ASM.

	N_1			N_7		
Iter$^{n.}$	$\mathcal{I}_l$	$\mathcal{I}_b$	$\mathcal{I}_u$	$\mathcal{I}_l$	$\mathcal{I}_b$	$\mathcal{I}_u$
0	0	474	0	0	10552	0
1	0	49	425	0	3350	7202
2	1	67	406	175	9573	804
3	8	171	295	438	9370	744
4	11	143	320	423	9346	783
5	13	140	321	437	9330	785
6	13	140	321	446	9322	784
7	13	140	321	447	9321	784
8	13	140	321	447	9321	784
9	13	140	321	447	9321	784

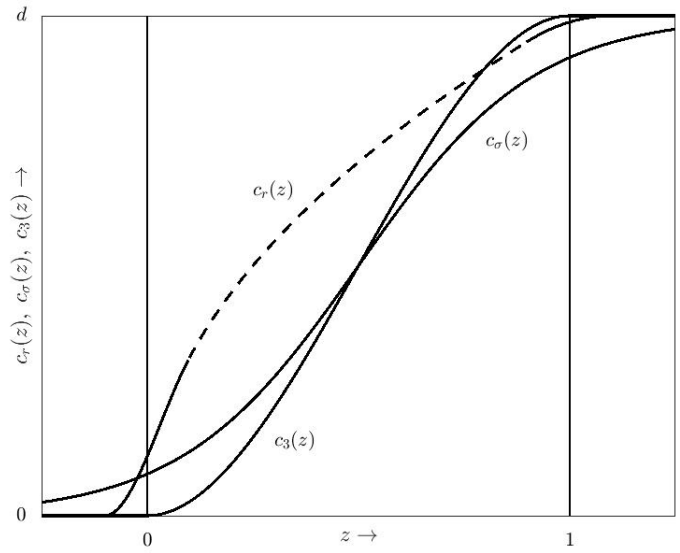

Figure 1: The cubic POR , $c_3(z)$, the logistic sigmoidal POR $c_\sigma(z)$ and the 2-side regularized Wagner POR , $c_r(z)$, (with exaggerated intervals of regularization). The dashed line in $c_r(z)$ is the original Wagner curve and the solid lines show the regularization cubics.

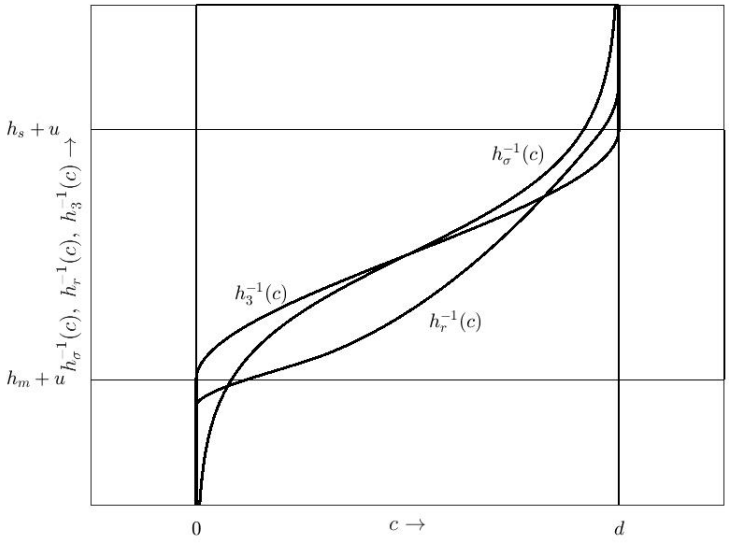

Figure 2: The inverses of the cubic, $h_3^{-1}(c)$, 2-side regularized Wagner, $h_r^{-1}(c)$, and logistic sigmoidal, $h_\sigma^{-1}(c)$, PORs . The inverses of the cubic and the 2-side regularized Wagner PORs have infinite derivatives at 0 and d and the inverse of the logistic sigmoidal POR is undefined at 0 and d.

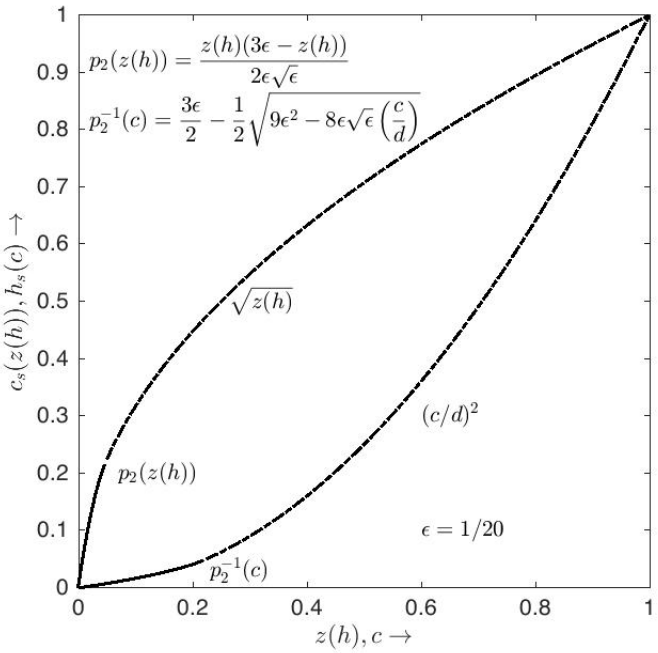

Figure 3: The 1-side regularized Wagner POR , $c_s(z(h))$ (with $\epsilon = 1/20$ and $d = 1$) and its inverse. The solid lines represent the quadratic component, $p_2(c)$, of the POR and of its inverse, $p_2^{-1}(c)$, and the dashed lines represent the original Wagner component, $\sqrt{z}$,and its inverse, $(c/d)^2$.

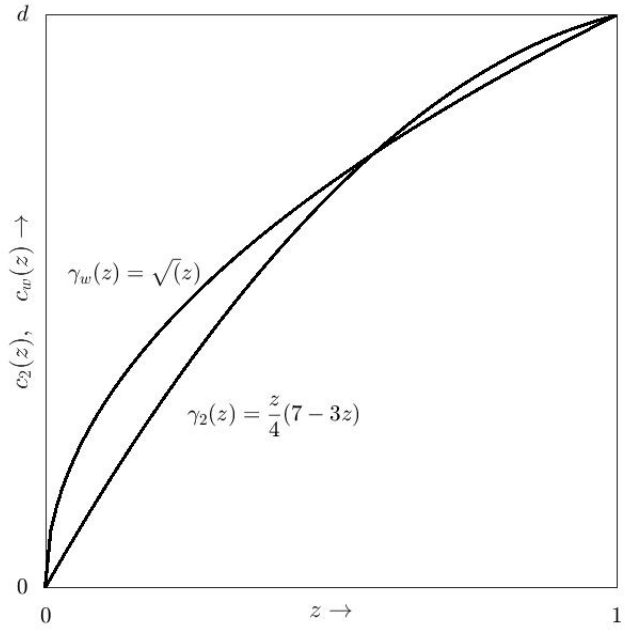

Figure 4: The new quadratic POR , $\gamma_2(z)$, (showing its finite derivative at $z = 0$) for $d = 1$ and the unregularized Wagner POR , $\gamma_w(z)$, (showing its infinite derivative at $z = 0$). The point-wise distance between the two curves $|c_2(z) - c_w(z)| < 0.15$ for $0 \leq z \leq 1$.

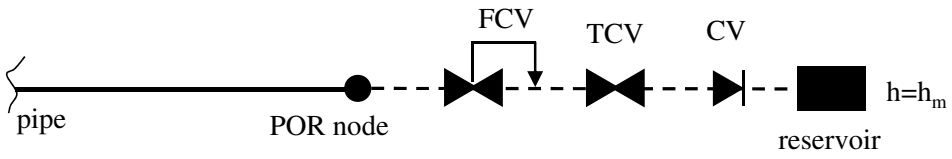

Figure 5: Using virtual elements (FCV, TCV, link with CV, reservoir) to model a pressure dependent node.

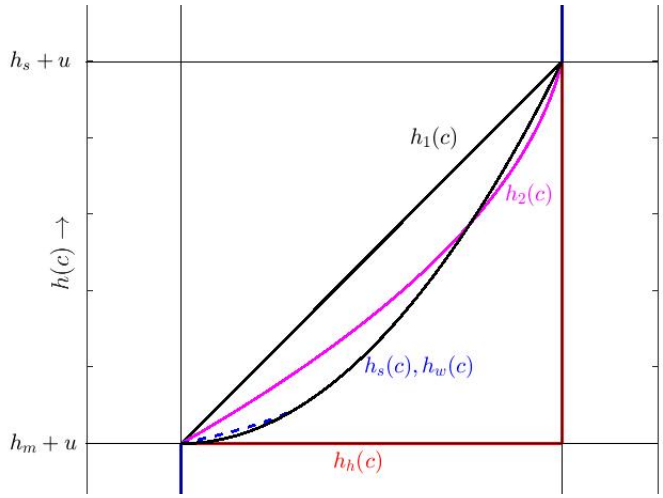

Figure 6: The multivalued, sub-differential mappings, $h(c)$, (derived from the inverse POR) given in (3) for the head expressed in terms of outflow for the linear, $h_1(c)$, quadratic, $h_2(c)$, 1-side regularized Wagner, $h_s(c)$, unregularized Wagner, $h_w(c)$ and Heaviside, $h_h(c)$, PORs . The dashed line depicts the quadratic component of $h_s(c)$. On the rest of the interval $h_s(c)$ overlays $h_w(c)$.

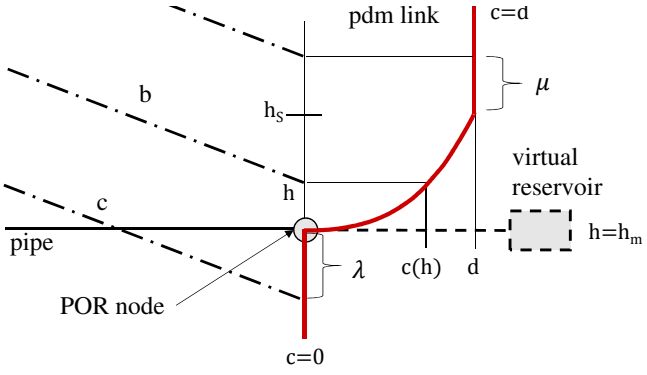

Figure 7: Illustration showing the physical meaning of some of the variables in the system (8)-(12)

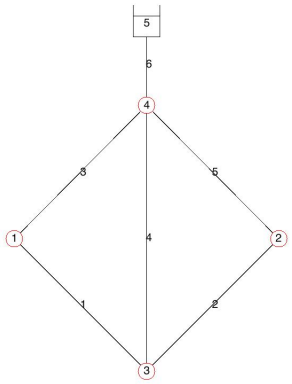

Figure 8: The example network used to illustrate the ASM.

List of Figures

List of Tables